The Computation of Conical Diffraction Coefficients in High-Frequency Acoustic Wave Scattering

B.D. Bonner*, I.G. Graham† and V.P. Smyshlyaev‡
Department of Mathematical Sciences
University of Bath, Bath BA2 7AY,
United Kingdom

July 7, 2003

Abstract

When a high-frequency acoustic or electromagnetic wave is scattered by a surface with a conical point, the component of the scattered wave corresponding to diffraction by the conical point can be represented as an asymptotic expansion, valid as the wave number $k \to \infty$. The *diffraction coefficient* is the coefficient of the principal term in this expansion. It can be computed by solving a family of homogeneous boundary value problems for the Laplace-Beltrami-Helmholtz equation (parametrised by a complex wave number-like parameter), on a portion of the unit sphere bounded by a simple closed contour ℓ, and then integrating the resulting solutions with respect to the complex parameter. In this paper we give the numerical analysis of a method for carrying out this computation (in the case of acoustic waves) via the boundary integral method applied on ℓ, emphasising the practically important case when the conical scatterer has lateral edges. The theory depends on an analysis of the integral equation on ℓ, which shows its relation to the corresponding integral equation for the planar Helmholtz equation. This allows us to prove optimal convergence for piecewise polynomial collocation methods of arbitrary order. We also discuss efficient quadrature techniques for assembling the boundary element matrices. We illustrate the theory with computations on the classical canonical open problem of a trihedral cone.

Keywords: Acoustic wave scattering, high-frequency asymptotics, diffraction coefficients, conical points, lateral edges, boundary integral method, collocation, mesh grading.

1 Introduction

When an incident plane acoustic or electromagnetic wave is scattered by a bounded impenetrable (3D) obstacle, the asymptotic behaviour of the scattered wave when the frequency is

*mapbdb@maths.bath.ac.uk
†I.G.Graham@bath.ac.uk
‡vps@maths.bath.ac.uk
This work was completed while the second author was visiting the programme on Computational Challenges in PDEs at the Newton Institute for Mathematical Sciences, Cambridge, UK.

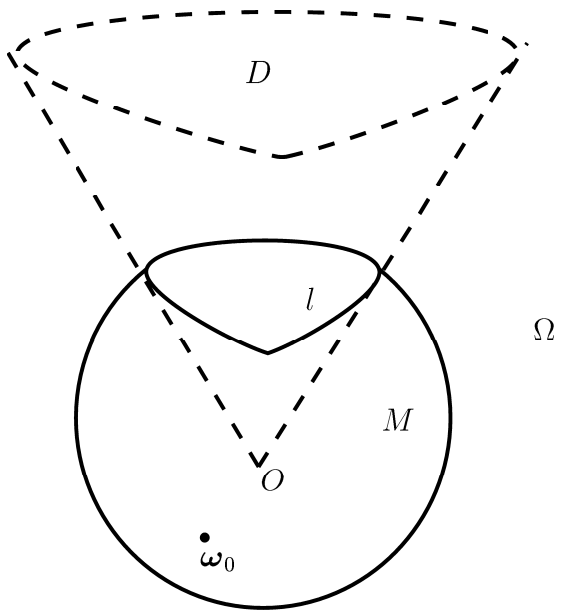

Figure 1: Geometry of obstacle

large is described by the classical Geometric Theory of Diffraction (GTD) [21]. As well as the simple reflections caused by a non-grazing incident wave at smooth parts of the obstacle, or a more complicated grazing incidence which leads to asymptotics in the shadow [20] and special boundary-layer asymptotics in the "penumbra" (see e.g. [6]), the scattered wave's asymptotics may also contain components arising from diffraction by non-smooth "singular" points of the scattering surface, such as edges or conical points. From the GTD [21] (and its further developments), the principal parts of those components are known to be described by the far field of waves scattered by the tangent cone at the singular point(s). This is the so-called "principle of localisation" (which is the essence of the GTD). Many authors have considered the problem of describing completely the asymptotics of the diffracted wave for various "canonical" cones (see e.g [7] and further references therein).

When the obstacle is a cone with a single conical point, this problem has been studied in detail by many authors, see e.g. [7],[5] and further references therein, where explicit formulae for the principal asymptotics of the diffracted wave were derived. For example, consider the scalar (acoustic) case, with an incident plane wave $U^{inc}(\mathbf{x}) = \exp(-ik\boldsymbol{\omega}_0 \cdot \mathbf{x})$, with the point $\boldsymbol{\omega}_0 \in S^2$, the unit sphere in $\mathbb{R}^3$, describing the direction of incidence. Then, both the scattered wave U^{sc} and the total wave $U := U^{inc} + U^{sc}$ satisfy the $3D$ Helmholtz equation, $(\Delta + k^2)U = 0$, in the domain of propagation, and U^{sc} satisfies an appropriate radiation condition. The theory in [23], [3] and [5] describes the behaviour of the diffracted component $U^{diff}(\mathbf{x})$ of $U^{sc}(\mathbf{x})$ at any point $\mathbf{x}$ in the domain of propagation. Using spherical coordinates centred at the conical point: $\mathbf{x} = r\boldsymbol{\omega}$ with $\boldsymbol{\omega} \in S^2$ and $r > 0$ denoting the distance of $\mathbf{x}$ from the conical point, it follows from the general recipes of the GTD that (with either Dirichlet or Neumann conditions imposed on the surface of the scatterer), U^{diff} has the asymptotic representation

$$U^{diff}(\mathbf{x}, k, \boldsymbol{\omega}_0) = 2\pi \frac{\exp(ikr)}{kr} f(\boldsymbol{\omega}, \boldsymbol{\omega}_0) + O((kr)^{-2}), \qquad k \to \infty. \tag{1.1}$$

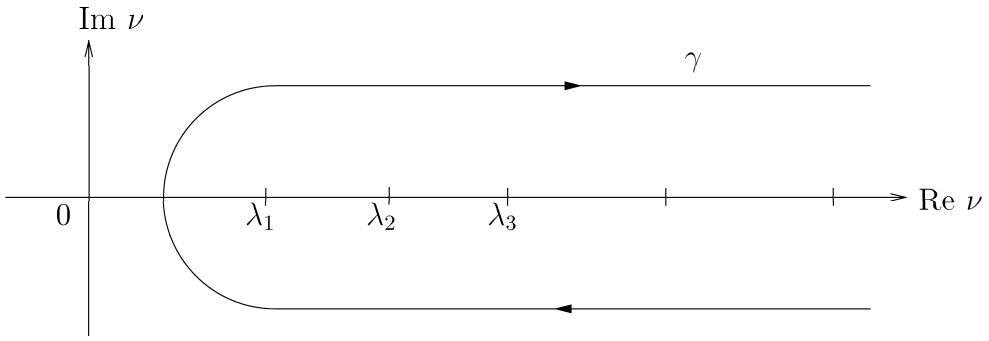

Figure 2: Contour of integration

Here the distribution $f(\boldsymbol{\omega}, \boldsymbol{\omega}_0)$, which is infinitely smooth everywhere except at the so-called "*singular directions*", is the important "*diffraction coefficient*" (also known as the kernel of the "*scattering matrix*"), and describes the intensity of the diffracted wave in the particular direction $\boldsymbol{\omega}$.

This paper is about the numerical analysis and implementation of methods for computing $f(\boldsymbol{\omega}, \boldsymbol{\omega}_0)$. In [3] and [5] an algorithm for this task was proposed.

To obtain a formula for f, we take O to be the vertex of the conical obstacle, Ξ, (which is indicated by dotted lines in Fig 1) and let M denote the portion of the unit sphere S^2 which is exterior to Ξ. M is a sub-manifold of S^2 with boundary which we denote by ℓ (see again Fig 1). Let Δ^* denote the Laplace-Beltrami operator on S^2 and introduce the "*spherical*" Green's function $g(\boldsymbol{\omega}, \boldsymbol{\omega}_0, \nu)$ on M, satisfying:

$$(\Delta^* + \nu^2 - 1/4)g(\boldsymbol{\omega}, \boldsymbol{\omega}_0, \nu) = \delta(\boldsymbol{\omega} - \boldsymbol{\omega}_0), \quad \boldsymbol{\omega}, \boldsymbol{\omega}_0 \in M \quad \text{and } \nu \in \mathbb{C}\ , \tag{1.2}$$

where δ denotes the Dirac delta function and the differentiation on the left-hand side is with respect to $\boldsymbol{\omega}$. As a function of $\boldsymbol{\omega}$, g is also required to satisfy a Dirichlet or Neumann boundary condition on ℓ (whichever is given in the original scattering problem). Once g is known, the diffraction coefficient in (1.1) is then given by the formula:

$$f(\boldsymbol{\omega}, \boldsymbol{\omega}_0) = \lim_{s \to 0} \frac{i}{\pi} \int_\gamma \exp(-i\nu(\pi + s)) g(\boldsymbol{\omega}, \boldsymbol{\omega}_0, \nu) \nu d\nu. \tag{1.3}$$

The integration contour γ in (1.3) has to be chosen in the complex plane, so that the (positive) numbers $\sqrt{\lambda}$ (where λ ranges over all eigenvalues of $-\Delta^* + 1/4$ on M, subject to the appropriate boundary condition on ℓ) lie on its right (see Fig 2).

Thus the computational procedure for realising the asymptotic formula (1.1) requires: (i) the computation of the Green's function $g(\boldsymbol{\omega}, \boldsymbol{\omega}_0, \nu)$ for all required incidence directions $\boldsymbol{\omega}_0$ and observation directions $\boldsymbol{\omega} \in M$ and (ii) the computation of the integral in (1.3), by quadrature. Note that (ii) in turn implies that $g(\boldsymbol{\omega}, \boldsymbol{\omega}_0, \nu)$ must be evaluated for sufficiently many $\nu \in \gamma$ to ensure an accurate answer.

For certain configurations of $\boldsymbol{\omega}, \boldsymbol{\omega}_0$ (which, say, in the case of a smooth, fully illuminated and convex cone corresponds to the direction of observation $\boldsymbol{\omega}$ with no reflected wave [23][3]), the right-hand side of (1.3) can be transformed by deforming the contour of integration γ onto the imaginary axis and then interchanging the limit with the integral. Moreover the Green's function g in (1.3) can be replaced by its regular part g^r, $g^r := g - g_0$, where g_0 is the

(known) fundamental solution for the operator $(\Delta^* + \nu^2 - 1/4)$ on all of S^2 (see §2). These modifications yield the simpler formula:

$$f(\boldsymbol{\omega}, \boldsymbol{\omega}_0) = -\frac{i}{\pi} \int_{-\infty}^{\infty} \exp(\tau\pi) g^r(\boldsymbol{\omega}, \boldsymbol{\omega}_0, i\tau) \tau d\tau. \tag{1.4}$$

The configurations of $\boldsymbol{\omega}$ and $\boldsymbol{\omega}_0$ for which the formulation (1.4) is possible are described by a geometrical condition (see [5, §2.3]). All our computations in this paper are for cases in which (1.4) is valid. In other cases one must compute the limit (1.3) as it stands, leading to a more complicated approximation problem directly employing (1.3) with sufficiently small s [5].

In [3] and [5] a numerical method was proposed for the computation of (1.4) and (1.3). The boundary integral method was used to compute g^r. (g^r satisfies the homogeneous PDE $(\Delta^* + \nu^2 - 1/4) g^r(\boldsymbol{\omega}, \boldsymbol{\omega}_0, \nu) = 0$, on the manifold M, subject to an inhomogeneous boundary condition on its boundary ℓ.) This was implemented in [3] and [5] in the case when Ξ is a smooth cone, using "in effect" a simple trapezoidal-Nyström type method and the trapezoidal rule was used for the contour integration with respect to ν in (1.3) or (1.4). The approach of [23],[3] and [5] was also extended to the electromagnetic case [24], which was implemented numerically in [4]. However the papers [3] and [5] contained no convergence analysis of the method and moreover, they dealt only with the case of a smooth cone Ξ. The case of a cone with lateral edges is of fundamental importance in both the high-frequency theory of diffraction (where it is one of the unsolved canonical problems [21]) and in practice, where high frequency scattering by antennae or corners of buildings is a key problem in microwave engineering.

Although the integral equation method reduces the computation of $g(\boldsymbol{\omega}, \boldsymbol{\omega}_0, \nu)$ to a computation on the (1D) contour ℓ on the surface of the unit sphere S^2, this equation has to be solved many times for different values of ν (and also more times if different $\boldsymbol{\omega}$ and $\boldsymbol{\omega}_0$ are to be considered). Moreover, as we shall see, the evaluation of the kernel in the integral equation arising from the spherical PDE (1.2) is much more costly than for typical boundary integral equations in planar scattering theory. Thus there is strong practical demand for the development of an efficient algorithm, in particular one which solves the integral equation with the highest accuracy and the minimal number of kernel evaluations. Thus the purposes of this paper are

(i) To propose an efficient method for computing diffraction coefficients which is robust even when the cone Ξ has lateral edges and analyse its convergence;

(ii) To minimise the number of kernel evaluations required in the implementation;

(iii) To demonstrate its use in the computation of diffraction coefficients in several sample cases.

The plan of the paper is as follows. In §2 we describe briefly the boundary integral method for computing g^r. This leads to non-standard integral equations posed on the spherical contour ℓ. In §3 we obtain the important properties of the integral operators which arise, including the case when the cone Ξ has lateral edges. In §4 we describe a flexible numerical method based on collocation with piecewise polynomials and we prove its convergence as a means of approximating $g^r(\boldsymbol{\omega}, \boldsymbol{\omega}_0, \nu)$. Finally in §5 we provide computations of diffraction coefficients for several sample problems. Subsequent work will consider the electromagnetic case. We also give §5 outline descriptions of various technical issues such as the computation of the contour

integral in (1.3) and the evaluation of the kernel which appears in the integral operator. These are described in more detail in [8].

2 Formulae for the Conical Diffraction Coefficients

Throughout the paper we shall assume that the cone Ξ has a finite number of smooth (analytic) faces, joined at lateral edges, and that the angle between pairs of adjacent faces lies in $(0, 2\pi)$ (i.e. cuspoid edges are excluded). This implies that the contour ℓ consists of a finite number of analytic arcs, also joined at non-cuspoid corners. For much of what we are going to do below, a lower order of smoothness for the faces would be sufficient, but we suppress this extra generality in the interests of readability.

For $\boldsymbol{\omega}, \boldsymbol{\omega}' \in S^2$ we define $\theta(\boldsymbol{\omega}, \boldsymbol{\omega}')$ to be the geodesic distance between two points $\boldsymbol{\omega}$ and $\boldsymbol{\omega}'$ on the sphere S^2 (i.e. $\cos\theta(\boldsymbol{\omega}, \boldsymbol{\omega}') = \boldsymbol{\omega} \cdot \boldsymbol{\omega}'$). We will assume that the cone satisfies

$$\theta(\boldsymbol{\omega}, \boldsymbol{\omega}') < \pi \quad \text{for all} \quad \boldsymbol{\omega}, \boldsymbol{\omega}' \in \ell. \tag{2.1}$$

This technical restriction, which is introduced for convenience could, in principle, be removed. However it holds for most practically important conical geometries. (An example of a case for which (2.1) fails is the three-dimensional wedge, consisting of two semi-infinite planes meeting on an infinite straight line. However the problem of diffraction by a wedge is solved by simpler methods.)

For a fully illuminated cone (i.e. $-\boldsymbol{\omega}_0 \notin M$) the technical condition alluded to in the introduction, which allows the deformation of the contour γ in (1.3) to the imaginary axis in (1.4) can now be stated as

$$\theta_1(\boldsymbol{\omega}, \boldsymbol{\omega}_0) = \min_{\boldsymbol{\omega} \in \ell} \{\theta(\boldsymbol{\omega}, \boldsymbol{\omega}') + \theta(\boldsymbol{\omega}', \boldsymbol{\omega}_0)\} > \pi. \tag{2.2}$$

when $\theta_1(\boldsymbol{\omega}, \boldsymbol{\omega}_0) \leq \pi$ the formula (1.3) may either be undefined or may have to be interpreted in a distributional sense. We will not discuss this here but the reader may refer to [5] and [8] for more detail, including the case when the cone is not fully illuminated.

As mentioned in §1, the regular part g^r of the Green's function g in (1.2) is defined by

$$g^r(\boldsymbol{\omega}, \boldsymbol{\omega}_0, \nu) = g(\boldsymbol{\omega}, \boldsymbol{\omega}_0, \nu) - g_0(\boldsymbol{\omega}, \boldsymbol{\omega}_0, \nu) \tag{2.3}$$

where g_0 is the fundamental solution:

$$g_0(\boldsymbol{\omega}, \boldsymbol{\omega}', \nu) = -\frac{1}{4\cos(\pi\nu)} P_{\nu - \frac{1}{2}}(-\cos\theta(\boldsymbol{\omega}, \boldsymbol{\omega}')), \tag{2.4}$$

with P_k denoting the Legendre special function of the first kind of index k (see e.g. [1, page 332]). It is well-known (see e.g. [23], [3], [5]) that this satisfies:

$$(\Delta^* + \nu^2 - 1/4) g_0(\boldsymbol{\omega}, \boldsymbol{\omega}', \nu) = \delta(\boldsymbol{\omega} - \boldsymbol{\omega}') \ , \quad \boldsymbol{\omega}, \boldsymbol{\omega}' \in S^2, \tag{2.5}$$

(where the differentiation is with respect to $\boldsymbol{\omega}$), i.e. it is the fundamental solution for the operator $\Delta^* + \nu^2 - 1/4$ on all of the sphere S^2. Comparing (2.5) and (1.2), we see that for each $\boldsymbol{\omega}_0 \in S^2$ and $\nu \in \mathbb{C}$, the function g^r, as a function of $\boldsymbol{\omega}$, satisfies the homogeneous PDE

$$(\Delta^* + \nu^2 - 1/4) g^r(\boldsymbol{\omega}, \boldsymbol{\omega}_0, \nu) = 0, \quad \boldsymbol{\omega} \in M, \tag{2.6}$$

subject to the boundary condition on ℓ

$$\left.\begin{array}{lll} \text{either} & g^r(\boldsymbol{\omega},\boldsymbol{\omega}_0,\nu) = -g_0(\boldsymbol{\omega},\boldsymbol{\omega}_0,\nu), & \text{the Dirichlet case} \\ \text{or} & (\partial g^r/\partial \mathbf{m})(\boldsymbol{\omega},\boldsymbol{\omega}_0,\nu) = -(\partial g_0/\partial \mathbf{m})(\boldsymbol{\omega},\boldsymbol{\omega}_0,\nu), & \text{the Neumann case} \end{array}\right\} \text{ for all } \boldsymbol{\omega} \in \ell\ . \tag{2.7}$$

The boundary condition to be imposed on g^r is inherited from the boundary condition imposed on the original scattering problem. In (2.7) and throughout the paper, $\partial/\partial\mathbf{m}$ denotes the (outward) normal derivative with respect to $\boldsymbol{\omega} \in \ell$, i.e. the derivative in the direction $\mathbf{m} \in S^2$ where $\mathbf{m}$ lies in the tangent plane to S^2 at $\boldsymbol{\omega} \in \ell$, is orthogonal to the tangent $\mathbf{t}$ at $\boldsymbol{\omega}$, and is directed outward from M.

The problem (2.6),(2.7) can now be solved by an integral equation method on ℓ. Here we follow the classical indirect approach, e.g. [2], adapted to the present problem in [3] and [5], although we note that a direct approach based on Green's formula would also be possible.

In the Dirichlet case, we seek the solution in the form of a double layer potential

$$g^r(\boldsymbol{\omega},\boldsymbol{\omega}_0,\nu) = \int_\ell \frac{\partial g_0}{\partial \mathbf{m}'}(\boldsymbol{\omega},\boldsymbol{\omega}',\nu)u(\boldsymbol{\omega}',\nu)d\boldsymbol{\omega}', \qquad \boldsymbol{\omega} \in M, \tag{2.8}$$

where $\partial/\partial\mathbf{m}'$ denotes the outward normal derivative at $\boldsymbol{\omega}' \in \ell$. Taking limits as $\boldsymbol{\omega}$ tends to the contour ℓ in (2.8) and using the jump conditions of the double layer potential and the Dirichlet boundary condition from (2.7), we obtain the second-kind integral equation:

$$\frac{1}{2}u(\boldsymbol{\omega},\nu) + \int_\ell \frac{\partial g_0}{\partial \mathbf{m}'}(\boldsymbol{\omega},\boldsymbol{\omega}',\nu)u(\boldsymbol{\omega}',\nu)d\boldsymbol{\omega}' = -g_0(\boldsymbol{\omega},\boldsymbol{\omega}_0,\nu), \tag{2.9}$$

for all smooth points $\boldsymbol{\omega} \in l$. This equation is given in [3]. A rigorous justification for potential theory on manifolds is given in a very general context in [12]. For corner points the factor $1/2$ has to be replaced by a factor related to the corner angle, c.f. [9]. However, since we will estimate errors for our boundary integral equations in L^2 type spaces, this point is unimportant. Notice that, since $\boldsymbol{\omega} \in \ell$ and $\boldsymbol{\omega}_0 \in M$, the right-hand side (2.9) is never singular.

Analogously, the Neumann problem is solved with the single layer potential:

$$g^r(\boldsymbol{\omega},\boldsymbol{\omega}_0,\nu) = \int_\ell g_0(\boldsymbol{\omega},\boldsymbol{\omega}',\nu)u(\boldsymbol{\omega}',\nu)d\boldsymbol{\omega}', \qquad \boldsymbol{\omega} \in M, \tag{2.10}$$

Taking the normal derivative and fitting the boundary condition leads to:

$$-\frac{1}{2}u(\boldsymbol{\omega},\nu) + \int_\ell \frac{\partial g_0}{\partial \mathbf{m}}(\boldsymbol{\omega},\boldsymbol{\omega}',\nu)u(\boldsymbol{\omega}',\nu)d\boldsymbol{\omega}' = -\frac{\partial g_0}{\partial \mathbf{m}}(\boldsymbol{\omega},\boldsymbol{\omega}_0,\nu), \tag{2.11}$$

We can write (2.9),(2.11) (almost everywhere) in operator form as

$$\Big(I + \mathcal{L}_B\Big)u = b_B\ , \quad \text{with } (\mathcal{L}_B u)(\boldsymbol{\omega}) = \int_\ell L_B(\boldsymbol{\omega},\boldsymbol{\omega}')u(\boldsymbol{\omega}')d\boldsymbol{\omega}'\ , \quad B = D, N, \tag{2.12}$$

with solution $u(\boldsymbol{\omega},\nu)$ abbreviated by $u(\boldsymbol{\omega})$. In the Dirichlet case the data is

$$b_D(\boldsymbol{\omega}) := -2g_0(\boldsymbol{\omega},\boldsymbol{\omega}_0,\nu)\ , \quad L_D(\boldsymbol{\omega},\boldsymbol{\omega}') := 2\frac{\partial g_0}{\partial \mathbf{m}'}(\boldsymbol{\omega},\boldsymbol{\omega}',\nu)\ , \tag{2.13}$$

and in the Neumann case,

$$b_N(\boldsymbol{\omega}) := 2\frac{\partial g_0}{\partial \mathbf{m}}(\boldsymbol{\omega},\boldsymbol{\omega}_0,\nu), \quad L_N(\boldsymbol{\omega},\boldsymbol{\omega}') := -2\frac{\partial g_0}{\partial \mathbf{m}}(\boldsymbol{\omega},\boldsymbol{\omega}',\nu)\ . \tag{2.14}$$

Although the operators in (2.12), with the kernels from (2.13) or (2.14) are not classical, we will show that their properties are analogous to those of the standard layer potentials for the Helmholtz equation on the boundary of a planar domain.

3 Integral Operators

3.1 Preliminary Results

The aim of this subsection is to identify the principal parts of the kernels L_D and L_N. This is done in Theorem 3.3. To prove this we need two technical lemmas.

Lemma 3.1

$$L_D(\boldsymbol{\omega},\boldsymbol{\omega}') = \frac{1}{2\cos(\pi\nu)}\, P'_{\nu-\frac{1}{2}}(-\cos\theta(\boldsymbol{\omega},\boldsymbol{\omega}'))\ \mathbf{t}'.(\boldsymbol{\omega}\wedge\boldsymbol{\omega}') \tag{3.1}$$

$$L_N(\boldsymbol{\omega},\boldsymbol{\omega}') = -\frac{1}{2\cos(\pi\nu)}\, P'_{\nu-\frac{1}{2}}(-\cos\theta(\boldsymbol{\omega},\boldsymbol{\omega}'))\ \mathbf{t}.(\boldsymbol{\omega}'\wedge\boldsymbol{\omega}) \tag{3.2}$$

where $\mathbf{t}$ *(respectively* $\mathbf{t}'$*) is the unit tangent to* ℓ *at* $\boldsymbol{\omega}$ *(respectively* $\boldsymbol{\omega}'$*) orientated such that* $\mathbf{t},\mathbf{m},\boldsymbol{\omega}$ *(respectively* $\mathbf{t}',\mathbf{m}',\boldsymbol{\omega}'$*) form an orthogonal right-handed triple (see Fig. 3 below).*

Proof First note that by employing spherical polar coordinates

$$\boldsymbol{\omega}' = (\sin\theta'\cos\phi', \sin\theta'\sin\phi', \cos\theta')^T,$$

then for any $v : S^2 \to \mathbb{R}$, we have the representation

$$\frac{\partial v}{\partial \mathbf{m}'}(\boldsymbol{\omega}') = \nabla_{\boldsymbol{\omega}'}\{v\circ\boldsymbol{\omega}'\}\cdot\mathbf{m}'\ ,$$

where $\nabla_{\boldsymbol{\omega}'}$ is the spherical gradient:

$$\nabla_{\boldsymbol{\omega}'} = \frac{1}{\sin\theta'}\mathbf{e}_{\phi'}\frac{\partial}{\partial\phi'} + \mathbf{e}_{\theta'}\frac{\partial}{\partial\theta'}\ ,$$

with

$$\mathbf{e}_{\phi'} = (-\sin\phi', \cos\phi', 0)^T \quad \text{and} \quad \mathbf{e}_{\theta'} = (\cos\theta'\cos\phi', \cos\theta'\sin\phi', -\sin\theta')^T\ .$$

Since $\cos\theta(\boldsymbol{\omega},\boldsymbol{\omega}') = \boldsymbol{\omega}\cdot\boldsymbol{\omega}'$, we have

$$\frac{\partial}{\partial\mathbf{m}'}P_{\nu-\frac{1}{2}}(-\cos\theta(\boldsymbol{\omega},\boldsymbol{\omega}')) = -P'_{\nu-\frac{1}{2}}(-\cos\theta(\boldsymbol{\omega},\boldsymbol{\omega}'))\ \nabla_{\boldsymbol{\omega}'}\Big\{\boldsymbol{\omega}\cdot\boldsymbol{\omega}'\Big\}\cdot\mathbf{m}'. \tag{3.3}$$

Now an easy calculation shows that

$$\nabla_{\boldsymbol{\omega}'}\Big\{\boldsymbol{\omega}\cdot\boldsymbol{\omega}'\Big\}\cdot\mathbf{m}' = \Big\{(\boldsymbol{\omega}\cdot\mathbf{e}_{\phi'})\ \mathbf{e}_{\phi'} + (\boldsymbol{\omega}\cdot\mathbf{e}_{\theta'})\ \mathbf{e}_{\theta'}\Big\}\cdot\mathbf{m}' = \boldsymbol{\omega}\cdot\mathbf{m}'.$$

Thus from (2.4) and (2.13), we have

$$L_D(\boldsymbol{\omega},\boldsymbol{\omega}') = \frac{1}{2\cos(\pi\nu)}\, P'_{\nu-\frac{1}{2}}(-\cos\theta(\boldsymbol{\omega},\boldsymbol{\omega}'))\ \boldsymbol{\omega}\cdot\mathbf{m}'\ . \tag{3.4}$$

Since $\mathbf{t}'$, $\mathbf{m}'$ and $\boldsymbol{\omega}'$ form a right-handed triple, we have $\mathbf{m}' = \boldsymbol{\omega}'\wedge\mathbf{t}'$, and so

$$L_D(\boldsymbol{\omega},\boldsymbol{\omega}') = \frac{1}{2\cos(\pi\nu)}\, P'_{\nu-\frac{1}{2}}(-\cos\theta(\boldsymbol{\omega},\boldsymbol{\omega}'))\ \boldsymbol{\omega}\cdot(\boldsymbol{\omega}'\wedge\mathbf{t}')\ ,$$

which is equivalent to (3.1) by cyclic permutation. Since $L_N(\boldsymbol{\omega},\boldsymbol{\omega}') = -L_D(\boldsymbol{\omega}',\boldsymbol{\omega})$, (3.2) follows easily. □

The next lemma identifies the asymptotic behaviour of $P'_{\nu+\frac{1}{2}}(x)$ for x close to -1. We will combine this with (3.1), (3.2) to identify the behaviour of L_D and L_N near $\boldsymbol{\omega} = \boldsymbol{\omega}'$.

Lemma 3.2 *For all $k \in \mathbb{C}$, $P_k(x)$ is an analytic function of $x \in (-1,1)$. Moreover*

$$P_k(x) = a_k(x) \log\left(\frac{1+x}{2}\right) + b_k(x),$$

where $a_k(x)$ and $b_k(x)$ are both analytic on $(-3,1)$, with

$$a_k(-1) = \frac{\sin(\pi k)}{\pi} \qquad \text{and} \qquad b_k(-1) = \frac{\sin(\pi k)}{\pi}\ \{\psi(k) + \psi(-k-1) + 2\gamma\},$$

where $\psi(k) = -\gamma - \sum_{r=1}^{\infty}(1/(k+r) - 1/r)$ and γ is the Euler constant.

Proof From [1, equation 8.1.2] we get the following representation of P_k

$$P_k(x) = F(-k, k+1; 1; \frac{1-x}{2}) \tag{3.5}$$

where F is the hypergeometric function. It follows from [1, page 556] that $F(-k, k+1; 1; z)$ is a convergent power series for $-1 \le z < 1$. Therefore, by (3.5), $P_k(x)$ is analytic for $x \in (-1,3)$ and in particular for $x \in (-1,1)$. This proves the first statement in the theorem.

Furthermore from [18, Chapter V. equation 53] we have that

$$P_k(x) = a_k(x) \log\left(\frac{1+x}{2}\right) + b_k(x),$$

where

$$a_k(x) = \frac{\sin(\pi k)}{\pi} F(-k, k+1; 1; (1+x)/2) \tag{3.6}$$

and

$$b_k(x) = \frac{\sin(\pi k)}{\pi}\left\{[\psi(k)+\psi(-k-1)+2\gamma]F(-k,k+1;1;(1+x)/2) + \sum_{r=1}^{\infty} B(k,r)\phi(k,r)\left(\frac{1+x}{2}\right)^r\right\}. \tag{3.7}$$

Here

$$B(k,r) = \frac{(-k)\dots(-k+r-1)(k+1)\dots(k+r)}{(r!)^2}$$

and

$$\phi(k,r) = \sum_{j=1}^{r}\left\{\frac{2k(k+1)+j}{(j^2-k^2-k-j)j}\right\}.$$

As remarked above, $F(-k, k+1; 1; (1+x)/2)$ is a convergent power series for $-1 \le (1+x)/2 < 1$, so $a_k(x)$ is analytic for $x \in (-3,1)$. Moreover $a_k(-1) = \sin(\pi k)/\pi$ follows from [1, page 556]).

Turning to b_k, it is clear that the first term on the right-hand side of (3.7) is also analytic for $x \in (-3,1)$ and that the assertions about b_k will then follow provided the domain of convergence of the power series

$$\sum_{r=1}^{\infty} B(k,r)\phi(k,r)\left(\frac{1+x}{2}\right)^r \tag{3.8}$$

can be shown to be $(-3,1)$.

To obtain this result, note that $\lim_{r\to\infty}\phi(k,r)$ is clearly finite. If $\lim_{r\to\infty}\phi(k,r)\neq 0$ then it follows that

$$\lim_{r\to\infty}\frac{|B(k,r+1)\ \phi(k,r+1)((1+x)/2)^{r+1}|}{|B(k,r)\ \phi(k,r)((1+x)/2)^{r}|}=\Big|\frac{1+x}{2}\Big|\lim_{r\to\infty}\Big|\frac{(-k+r)(k+r+1)}{(r+1)^2}\frac{\phi(k,r+1)}{\phi(k,r)}\Big|$$
$$=\Big|\frac{1+x}{2}\Big|, \tag{3.9}$$

and (3.8) is convergent for $x\in(-3,1)$ by the ratio test. However if $\lim_{r\to\infty}\phi(k,r)=0$ then, for large enough r, $|\phi(k,r)|<1$. Since (3.9) also shows that the power series $\sum_{r=1}^{\infty}B(k,r)((1+x)/2)^r$ converges for $x\in(-3,1)$, the comparison test then ensures that (3.8) also converges for $x\in(-3,1)$.

□

We now combine Lemmas 3.1 and 3.2 to obtain:

Theorem 3.3 *(i) For $\boldsymbol{\omega},\boldsymbol{\omega}'\in\ell$,*

$$L_D(\boldsymbol{\omega},\boldsymbol{\omega}')=-\frac{\mathbf{t}'\cdot(\boldsymbol{\omega}\wedge\boldsymbol{\omega}')}{\pi|\boldsymbol{\omega}-\boldsymbol{\omega}'|^2}+F_D(\boldsymbol{\omega},\boldsymbol{\omega}'), \tag{3.10}$$

$$L_N(\boldsymbol{\omega},\boldsymbol{\omega}')=\frac{\mathbf{t}\cdot(\boldsymbol{\omega}'\wedge\boldsymbol{\omega})}{\pi|\boldsymbol{\omega}-\boldsymbol{\omega}'|^2}+F_N(\boldsymbol{\omega},\boldsymbol{\omega}'), \tag{3.11}$$

where F_D and F_N are bounded on $\ell\times\ell$.

(ii) When $\boldsymbol{\omega}$ is not a corner point of ℓ,

$$\frac{\mathbf{t}'\cdot(\boldsymbol{\omega}\wedge\boldsymbol{\omega}')}{\pi|\boldsymbol{\omega}-\boldsymbol{\omega}'|^2}\quad\textit{and}\quad\frac{\mathbf{t}\cdot(\boldsymbol{\omega}'\wedge\boldsymbol{\omega})}{\pi|\boldsymbol{\omega}-\boldsymbol{\omega}'|^2} \tag{3.12}$$

are both smooth functions of $\boldsymbol{\omega}'$ in a neighbourhood of $\boldsymbol{\omega}$ and, for $B=D$ or N,

$$F_B(\boldsymbol{\omega},\boldsymbol{\omega}')=O(|\boldsymbol{\omega}-\boldsymbol{\omega}'|^2\log|\boldsymbol{\omega}-\boldsymbol{\omega}'|)\ ,\quad \textit{as}\quad \boldsymbol{\omega}'\to\boldsymbol{\omega}\ . \tag{3.13}$$

Proof We give the proof for L_D; the argument for L_N is analogous.

(i) From Lemma 3.2 with $k=\nu-1/2$, we have, for $x>-1$,

$$P'_{\nu-\frac12}(x)=\frac{-\cos(\pi\nu)}{\pi}\left\{\frac{1}{x+1}\right\}+r(x) \tag{3.14}$$

where

$$r(x)=\left[\frac{a_{\nu-\frac12}(x)-a_{\nu-\frac12}(-1)}{x-(-1)}+a'_{\nu-\frac12}(x)\log\left(\frac{x+1}{2}\right)+b'_{\nu-\frac12}(x)\right]\ . \tag{3.15}$$

Also note that, since $\boldsymbol{\omega},\boldsymbol{\omega}'\in S^2$, we have

$$-\cos\theta(\boldsymbol{\omega},\boldsymbol{\omega}')+1=-\boldsymbol{\omega}.\boldsymbol{\omega}'+1=\frac12|\boldsymbol{\omega}-\boldsymbol{\omega}'|^2\ . \tag{3.16}$$

Hence

$$P'_{\nu-\frac12}(-\cos\theta(\boldsymbol{\omega},\boldsymbol{\omega}'))=-\frac{2\cos(\pi\nu)}{\pi|\boldsymbol{\omega}-\boldsymbol{\omega}'|^2}+r(-1+|\boldsymbol{\omega}-\boldsymbol{\omega}'|^2/2). \tag{3.17}$$

Therefore combining Lemma 3.1 with (3.15) and (3.17), we obtain the formula (3.10) where

$$F_D(\boldsymbol{\omega},\boldsymbol{\omega}') = \frac{1}{2\cos(\pi\nu)}\; r(-1+|\boldsymbol{\omega}-\boldsymbol{\omega}'|^2/2)\; \mathbf{t}'\cdot(\boldsymbol{\omega}\wedge\boldsymbol{\omega}')\;. \tag{3.18}$$

To complete the proof of (i) we now show that F_D is bounded on $\ell\times\ell$. Substituting (3.15) into (3.18) we obtain

$$\begin{aligned} &2\cos(\pi\nu)F_D(\boldsymbol{\omega},\boldsymbol{\omega}') = \\ &\mathbf{t}'\cdot(\boldsymbol{\omega}\wedge\boldsymbol{\omega}')\left\{\frac{a_{\nu-\frac12}(-1+|\boldsymbol{\omega}-\boldsymbol{\omega}'|^2/2)-a_{\nu-\frac12}(-1)}{|\boldsymbol{\omega}-\boldsymbol{\omega}'|^2/2}+\; b'_{\nu-\frac12}(-1+|\boldsymbol{\omega}-\boldsymbol{\omega}'|^2/2)\right\} \qquad (3.19)\\ &+\; a'_{\nu-\frac12}(-1+|\boldsymbol{\omega}-\boldsymbol{\omega}'|^2/2)\;\left\{\mathbf{t}'\cdot(\boldsymbol{\omega}\wedge\boldsymbol{\omega}')\log(|\boldsymbol{\omega}-\boldsymbol{\omega}'|^2/4)\right\}\;. \qquad (3.20)\end{aligned}$$

To obtain the desired result for F_D, recall from Lemma 3.2 that $a_{\nu-\frac12}$ and $b'_{\nu-\frac12}$ are both analytic on $(-3,1)$. Also, using the assumption (2.1) and the compactness of ℓ, it follows that there exists $\epsilon>0$ such that $-1\le-\cos\theta(\boldsymbol{\omega},\boldsymbol{\omega}')\le 1-\epsilon$, for all $\boldsymbol{\omega},\boldsymbol{\omega}'\in\ell$. Thus it follows from (3.16) that

$$-1\le -1+|\boldsymbol{\omega}-\boldsymbol{\omega}|^2/2\le 1-\epsilon. \tag{3.21}$$

Since $|\boldsymbol{\omega}-\boldsymbol{\omega}'|^2$ is a smooth function of $\boldsymbol{\omega},\boldsymbol{\omega}'$, it follows that the terms inside the braces in (3.19) are smooth functions of $\boldsymbol{\omega},\boldsymbol{\omega}'\in\ell$. Moreover

$$\begin{aligned} |\mathbf{t}'\cdot(\boldsymbol{\omega}\wedge\boldsymbol{\omega}')|\le|\mathbf{t}'||\boldsymbol{\omega}\wedge\boldsymbol{\omega}'| &= \sin\theta(\boldsymbol{\omega},\boldsymbol{\omega}')=\{1-\cos^2\theta(\boldsymbol{\omega},\boldsymbol{\omega}')\}^{1/2}\\ &= \{1-(\boldsymbol{\omega}\cdot\boldsymbol{\omega}')^2\}^{1/2}=\{(1-\boldsymbol{\omega}\cdot\boldsymbol{\omega}')(1+\boldsymbol{\omega}\cdot\boldsymbol{\omega}')\}^{1/2}\\ &= \frac12|\boldsymbol{\omega}-\boldsymbol{\omega}'||\boldsymbol{\omega}+\boldsymbol{\omega}'|. \end{aligned} \tag{3.22}$$

which ensures the boundedness of (3.19). The boundedness of (3.20) follows in a similar way, using the above remarks and the analyticity of $a'_{\nu-\frac12}$ on $(-3,1)$.

(ii) Now suppose that $\boldsymbol{\omega}$ is not a corner point and that $\boldsymbol{\omega}'$ is sufficiently close to $\boldsymbol{\omega}$ so as to ensure that there is no corner point between $\boldsymbol{\omega}$ and $\boldsymbol{\omega}'$ on ℓ. Let $\boldsymbol{\rho}$ denote an arclength parameterisation of ℓ from any fixed reference point, set $\boldsymbol{\omega}=\boldsymbol{\rho}(s)$ and choose the parameterisation such that the unit tangent $\mathbf{t}$ at $\boldsymbol{\omega}$ is given by $\mathbf{t}=\boldsymbol{\rho}_s(s)$, the derivative of $\boldsymbol{\rho}(s)$. Then for $\boldsymbol{\omega}'$ near $\boldsymbol{\omega}$ with $\boldsymbol{\omega}'=\boldsymbol{\rho}(\sigma)$, we have

$$|\boldsymbol{\omega}-\boldsymbol{\omega}'|/|s-\sigma|=O(1)\quad\text{and}\quad|s-\sigma|/|\boldsymbol{\omega}-\boldsymbol{\omega}'|=O(1)\qquad\text{as }\;\sigma\to s. \tag{3.23}$$

Also,

$$\boldsymbol{\omega}\wedge\boldsymbol{\omega}'=\boldsymbol{\rho}(s)\wedge\boldsymbol{\rho}(\sigma)=(\boldsymbol{\rho}(s)-\boldsymbol{\rho}(\sigma))\wedge\boldsymbol{\rho}(\sigma).$$

Hence

$$\mathbf{t}'\cdot(\boldsymbol{\omega}\wedge\boldsymbol{\omega}')=\boldsymbol{\rho}_s(\sigma)\cdot((\boldsymbol{\rho}(s)-\boldsymbol{\rho}(\sigma)-(s-\sigma)\boldsymbol{\rho}_s(\sigma))\wedge\boldsymbol{\rho}(\sigma)). \tag{3.24}$$

Since $|\boldsymbol{\omega}-\boldsymbol{\omega}'|^2=(\boldsymbol{\rho}(s)-\boldsymbol{\rho}(\sigma))\cdot(\boldsymbol{\rho}(s)-\boldsymbol{\rho}(\sigma))$, it follows that (3.12) are smooth functions as $\sigma\to s$ (i.e. $\boldsymbol{\omega}'\to\boldsymbol{\omega}$). Moreover (3.23) and (3.24) imply that $|\mathbf{t}'\cdot(\boldsymbol{\omega}\wedge\boldsymbol{\omega}')|=O(|\boldsymbol{\omega}-\boldsymbol{\omega}'|^2)$ and so (3.13) follows from (3.20). □

We see from Theorem 3.3 that if there are no corner points on ℓ, then L_D and L_N are bounded (in fact continuous), so in both the Dirichlet and Neumann cases the integral operator $\mathcal{L}_B$ will be compact on most standard spaces, e.g. $C(\ell), L^2(\ell)$. Then standard stability proofs

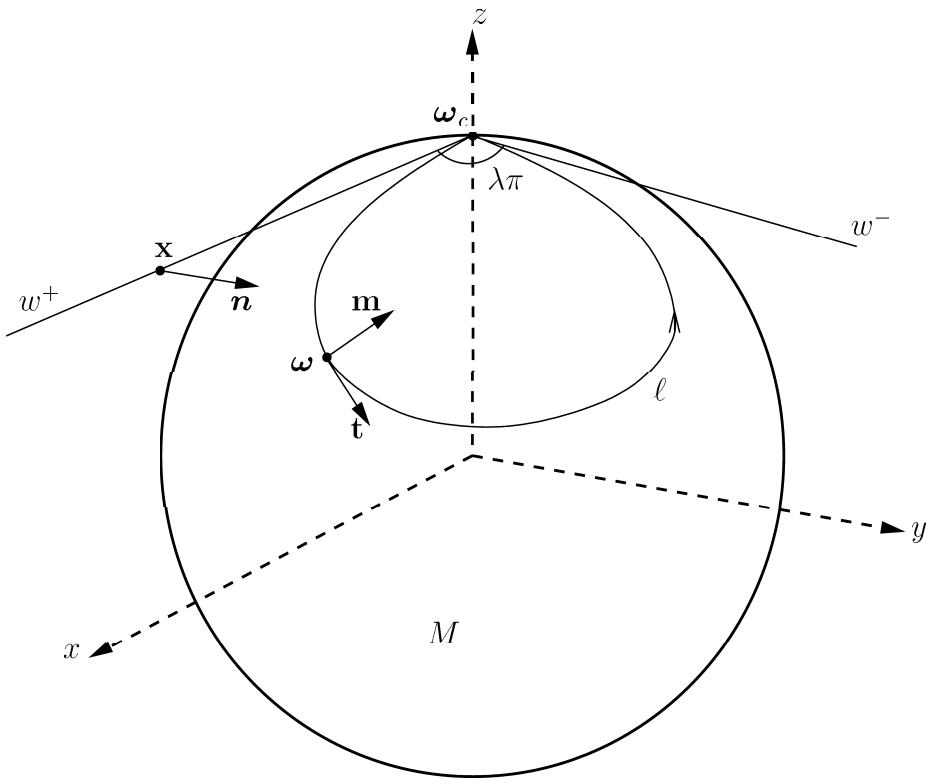

Figure 3: Wedge w and contour ℓ

for the numerical method will follow. However if ℓ does contain a corner, compactness is lost and so another approach is needed to show stability of a numerical method. The approach we will use is to compare the integral operator $\mathcal{L}_B$ with a corresponding plane Laplace integral operator $\mathcal{K}_B$ and then use stability results which are known for the planar Laplace problem. This is done in the following subsection.

3.2 Relation to Planar Laplace Case

To simplify the presentation, we assume that the contour ℓ has one corner which we will denote by the point $\boldsymbol{\omega}_c \in S^2$. The case of several corners is obtained analogously. Without loss of generality, we assume $\boldsymbol{\omega}_c = (0,0,1)^T$. Let $\boldsymbol{\rho}$ denote the arclength parameterisation of ℓ chosen so that $\boldsymbol{\rho}(0) = \boldsymbol{\omega}_c$ and so that $\boldsymbol{\rho}(s)$ travels around ℓ with M on the right-hand side (as indicated by the arrow in Fig. 3), as s travels from $-\Lambda$ to Λ, where 2Λ is the length of ℓ. Then we can introduce the "*wedge*" w in the tangent plane to S^2 at $\boldsymbol{\omega}_c$ as follows.

Definition 3.4 *The wedge w is defined to be the union of two straight line segments: $w{=}w^- \cup w^+$ where*

$$w^- = \{(0,0,1)^T + s\mathbf{t}_c^- : s \in [-\Lambda, 0]\}, \qquad w^+ = \{(0,0,1)^T + s\mathbf{t}_c^+ : s \in [0, \Lambda]\},$$

and $\mathbf{t}_c^\pm = \lim_{s\to 0\pm} \boldsymbol{\rho}_s(s)$ (see Fig. 3). The angle between the tangents $\mathbf{t}_c^+$ and $-\mathbf{t}_c^-$ is measured "anticlockwise" about the z axis (when viewed from outside the sphere) from w^+ to w^- and is denoted $\lambda\pi$, where $\lambda \in (0,2)\backslash\{1\}$. Without loss of generality we choose our coordinate system so that $\mathbf{t}_c^+$ is in the direction of the x axis. Each $\mathbf{x} = s\mathbf{t}_c^\pm \in w^\pm$ can be associated with a unique

$\boldsymbol{\omega} = \boldsymbol{\rho}(s) \in \ell$, and with a unit normal $\mathbf{m}$ at $\boldsymbol{\omega} \in \ell$ orientated outward from M. To $\mathbf{x}$ we associate a unit normal $\boldsymbol{n}$ to w in the plane tangent to S^2 at $\boldsymbol{\omega}_c$, orientated so that $\boldsymbol{n} \cdot \mathbf{m} \to 1$ as $s \to 0$. (See also Fig 3.)

The fundamental solution of Laplace's equation on the plane is $(1/2\pi)\log|\mathbf{x}-\mathbf{x}'|$. Using this we introduce the operators

$$(\mathcal{K}_B u)(\mathbf{x}) = \int_w K_B(\mathbf{x},\mathbf{x}')u(\mathbf{x}')d\mathbf{x}' \ , B = D, N \ .$$

Analogously to (2.13), (2.14), the Dirichlet and Neumann kernels are

$$K_D(\mathbf{x},\mathbf{x}') := \frac{1}{\pi}\frac{\partial}{\partial \boldsymbol{n}'}\{\log|\mathbf{x}-\mathbf{x}'|\} = -\frac{(\mathbf{x}-\mathbf{x}')\cdot \boldsymbol{n}'}{\pi|\mathbf{x}-\mathbf{x}'|^2} \tag{3.25}$$

$$K_N(\mathbf{x},\mathbf{x}') := -\frac{1}{\pi}\frac{\partial}{\partial \boldsymbol{n}}\{\log|\mathbf{x}-\mathbf{x}'|\} = -\frac{(\mathbf{x}-\mathbf{x}')\cdot \boldsymbol{n}}{\pi|\mathbf{x}-\mathbf{x}'|^2}. \tag{3.26}$$

Here $\boldsymbol{n}, \boldsymbol{n}'$ are unit normals to $\boldsymbol{\omega}$ at $\mathbf{x}, \mathbf{x}' \in w$, as described in Definition 3.4.

Theorem 3.5 will show that the principal singularity of L_B near $\boldsymbol{\omega} = \boldsymbol{\omega}' = \boldsymbol{\omega}_c$ is the same as K_B near $\mathbf{x} = \mathbf{x}' = \boldsymbol{\omega}_c$. This is useful because the properties of the integral operator $\mathcal{K}_B$ with kernel K_B are well-understood [11], [9], [15].

To prepare for Theorem 3.5, we use the arclength parameterisation, $\boldsymbol{\rho}(\sigma)$, of ℓ, introduced above, to rewrite (2.12) on $[-\Lambda, \Lambda]$. Putting $\boldsymbol{\omega} = \boldsymbol{\rho}(s)$ and $\boldsymbol{\omega}' = \boldsymbol{\rho}(\sigma)$ we obtain

$$(I + \widehat{\mathcal{L}}_B)\widehat{u} = \widehat{b}_B \ , \ \text{ with } \ (\widehat{\mathcal{L}}_B\widehat{u})(s) = \int_{-\Lambda}^{\Lambda} \widehat{L}_B(s,\sigma)\widehat{u}(\sigma)d\sigma, \quad s \in [-\Lambda, \Lambda], \tag{3.27}$$

where $\widehat{u}(s) = u(\boldsymbol{\rho}(s))$. In the case of Dirichlet boundary data, using (2.13) and Lemma 3.1 we have

$$\begin{aligned} &\widehat{b}_D(s) := -2g_0(\boldsymbol{\rho}(s), \boldsymbol{\omega}_0, \nu) \quad \text{and} \\ &\widehat{L}_D(s,\sigma) := \frac{1}{2\cos(\pi\nu)}\ P'_{\nu-\frac{1}{2}}(-\cos\theta(\boldsymbol{\rho}(s),\boldsymbol{\rho}(\sigma)))\ \boldsymbol{\rho}_s(\sigma)\cdot(\boldsymbol{\rho}(s)\wedge\boldsymbol{\rho}(\sigma)). \end{aligned} \tag{3.28}$$

(Note that since $\boldsymbol{\rho}$ is the arclength parameterisation, the Jacobian satisfies $|\boldsymbol{\rho}_s(\sigma)| = 1$ and does not appear explicitly in the kernel.) For Neumann boundary data, using (2.14) and Lemma 3.1 we obtain,

$$\begin{aligned} &\widehat{b}_N(s) := 2\frac{\partial g_0}{\partial \mathbf{m}(s)}(\boldsymbol{\rho}(s), \boldsymbol{\omega}_0, \nu) \quad \text{and} \\ &\widehat{L}_N(s,\sigma) := -\frac{1}{2\cos(\pi\nu)}\ P'_{\nu-\frac{1}{2}}(-\cos\theta(\boldsymbol{\rho}(s),\boldsymbol{\rho}(\sigma)))\ \boldsymbol{\rho}_s(s)\cdot(\boldsymbol{\rho}(\sigma)\wedge\boldsymbol{\rho}(s)), \end{aligned} \tag{3.29}$$

where $\mathbf{m}(s)$ is the corresponding normal to ℓ at $\boldsymbol{\rho}(s)$.

If we now denote the arclength parameterisation of w by $\boldsymbol{r}$, with $\boldsymbol{r}(-\Lambda) = (0,0,1)^T - \Lambda\mathbf{t}_c^-$, $\boldsymbol{r}(0) = \boldsymbol{\omega}_c$ and $\boldsymbol{r}(\Lambda) = (0,0,1)^T + \Lambda\mathbf{t}_c^+$, then we can also rewrite $\mathcal{K}_B$ as an operator

$$(\widehat{\mathcal{K}}_B\widehat{u})(s) = \int_{-\Lambda}^{\Lambda} \widehat{K}_B(s,\sigma)\widehat{u}(\sigma)d\sigma \qquad s \in [-\Lambda, \Lambda] \ , \quad B = D, N \ ,$$

where from (3.25), (3.26),

$$\widehat{K}_D(s,\sigma) := -\frac{(\boldsymbol{r}(s)-\boldsymbol{r}(\sigma))\cdot\boldsymbol{n}(\sigma)}{\pi|\boldsymbol{r}(s)-\boldsymbol{r}(\sigma)|^2}, \tag{3.30}$$

$$\widehat{K}_N(s,\sigma) := -\frac{(\boldsymbol{r}(s)-\boldsymbol{r}(\sigma))\cdot\boldsymbol{n}(s)}{\pi|\boldsymbol{r}(s)-\boldsymbol{r}(\sigma)|^2}, \tag{3.31}$$

for the Dirichlet and Neumann problems respectively. Here $\boldsymbol{n}(\sigma)$ is the normal to w at $\mathbf{x}=\boldsymbol{r}(\sigma)$. The following theorem shows that $\widehat{K}_B$ contains the principal singularity of $\widehat{L}_B$ near the corner point $s=\sigma=0$ in both the Dirichlet and Neumann cases, $B=D,N$.

Theorem 3.5 *Let $B=D$ or N. Then for $(s,\sigma)\in[-\Lambda,\Lambda]\times[-\Lambda,\Lambda]$, $\widehat{L}_B(s,\sigma)-\widehat{K}_B(s,\sigma)$ is a bounded function.*

Proof We give the proof for the case $B=D$. The case $B=N$ is analogous. First we consider the kernel $\widehat{K}_D$. From Definition 3.4 the parametric equation, $\boldsymbol{r}$, for w, is given by

$$\boldsymbol{r}(\sigma)=\begin{cases}(-\sigma\cos(\lambda\pi),-\sigma\sin(\lambda\pi),1)^T, & \sigma\in[-\Lambda,0]\\ (\sigma,0,1)^T, & \sigma\in[0,\Lambda].\end{cases} \tag{3.32}$$

Notice that if $-\Lambda\le s,\sigma\le 0$ or $0\le s,\sigma\le\Lambda$ then $\boldsymbol{r}(s)$ and $\boldsymbol{r}(\sigma)$ lie on the same arm of w and so it follows from (3.30) that $\widehat{K}_D(s,\sigma)=0$ and, by Theorem 3.3(ii), $\widehat{L}_D(s,\sigma)$ is bounded. So we have to consider only the case when s and σ are on different sides of 0.

First consider the case $-\Lambda\le s\le 0\le\sigma\le\Lambda$. Then (3.32) implies that $\boldsymbol{r}(s)-\boldsymbol{r}(\sigma)=(-s\cos(\lambda\pi)-\sigma,-s\sin(\lambda\pi),0)^T$ and $\boldsymbol{n}(\sigma)=(0,1,0)^T$. Therefore $(\boldsymbol{r}(s)-\boldsymbol{r}(\sigma))\cdot\boldsymbol{n}(\sigma)=-s\sin(\lambda\pi)$ and $|\boldsymbol{r}(s)-\boldsymbol{r}(\sigma)|^2=s^2+2s\sigma\cos(\lambda\pi)+\sigma^2$. So from (3.30),

$$\widehat{K}_D(s,\sigma)=\frac{1}{\pi}\frac{s\sin(\lambda\pi)}{(s^2+2s\sigma\cos(\lambda\pi)+\sigma^2)},\quad -\Lambda\le s\le 0\le\sigma\le\Lambda. \tag{3.33}$$

A similar calculation shows analogously that

$$\widehat{K}_D(s,\sigma)=-\frac{1}{\pi}\frac{s\sin(\lambda\pi)}{(s^2+2s\sigma\cos(\lambda\pi)+\sigma^2)},\quad -\Lambda\le\sigma\le 0\le s\le\Lambda. \tag{3.34}$$

Now we turn our attention to the kernel, $\widehat{L}_D(s,\sigma)$. Using Taylor's theorem we can write the parameterisation $\boldsymbol{\rho}$ as,

$$\boldsymbol{\rho}(\sigma)=\begin{cases}(-\sigma\cos(\lambda\pi),-\sigma\sin(\lambda\pi),1)^T+\sigma^2(\alpha_1(-\sigma),\beta_1(-\sigma),\gamma_1(-\sigma))^T, & \sigma\in[-\Lambda,0]\\ (\sigma,0,1)^T+\sigma^2(\alpha_2(\sigma),\beta_2(\sigma),\gamma_2(\sigma))^T, & \sigma\in[0,\Lambda],\end{cases} \tag{3.35}$$

where $\alpha_i(s),\beta_i(s)$ and $\gamma_i(s)$ are smooth functions on $[0,\Lambda]$, for $i=1,2$. Thus, for $-\Lambda\le s\le 0\le\sigma\le\Lambda$, we have, from (3.35),

$$\boldsymbol{\rho}(s)\wedge\boldsymbol{\rho}(\sigma)=(-s\sin(\lambda\pi),s\cos(\lambda\pi)+\sigma,0)^T+O(\max\{|s|,|\sigma|\}^2),$$

as $\max\{|s|,|\sigma|\}\to 0$. Hence with $\boldsymbol{\omega}=\boldsymbol{\rho}(s)$ and $\boldsymbol{\omega}'=\boldsymbol{\rho}(\sigma)$, we have

$$\mathbf{t}'=\boldsymbol{\rho}_s(\sigma) = (1,0,0)^T+O(|\sigma|)\ , \tag{3.36}$$

$$-\mathbf{t}'\cdot(\boldsymbol{\omega}\wedge\boldsymbol{\omega}') = s\sin(\lambda\pi)+O(\max\{|s|,|\sigma|\}^2)$$

$$\text{and}\quad |\boldsymbol{\omega}-\boldsymbol{\omega}'|^2 = s^2+2s\sigma\cos(\lambda\pi)+\sigma^2+O(\max\{|s|,|\sigma|\}^3)\ , \tag{3.37}$$

as $\max\{|s|,|\sigma|\} \to 0$. Therefore we have from (3.10)

$$\widehat{L}_D(s,\sigma) = \frac{\sin(\lambda\pi)}{\pi} \frac{s+\eta_2(s,\sigma)}{s^2+2s\sigma\cos(\lambda\pi)+\sigma^2+\eta_3(s,\sigma)} + \widehat{F}_D(s,\sigma),$$

where $\widehat{F}_D(s,\sigma) = F_D(\boldsymbol{\rho}(s),\boldsymbol{\rho}(\sigma))$ and

$$\eta_i(s,\sigma) = O(\max\{|s|,|\sigma|\}^i), \quad i=2,3. \tag{3.38}$$

Hence, for $-\Lambda \le s \le 0 \le \sigma \le \Lambda$,

$$(\widehat{L}_D - \widehat{K}_D)(s,\sigma) = \frac{\sin(\lambda\pi)}{\pi}\left\{ \frac{s+\eta_2(s,\sigma)}{s^2+2s\sigma\cos(\lambda\pi)+\sigma^2+\eta_3(s,\sigma)} - \frac{s}{s^2+2s\sigma\cos(\lambda\pi)+\sigma^2} \right\} + \widehat{F}_D(s,\sigma), \tag{3.39}$$

which is clearly continuous for $(s,\sigma) \neq (0,0)$.

In order to show that $(\widehat{L}_D - \widehat{K}_D)(s,\sigma)$ is bounded near $(s,\sigma)=(0,0)$ we need to show that the limit (as $(s,\sigma)\to(0,0)$) of the first term on the right-hand side of (3.39) is bounded. We do this for $0 < -s \le \sigma$. The case $0 < \sigma \le -s$ is analogous. To obtain the result, write

$$\begin{aligned} &\frac{s+\eta_2(s,\sigma)}{s^2+2s\sigma\cos(\lambda\pi)+\sigma^2+\eta_3(s,\sigma)} - \frac{s}{s^2+2s\sigma\sin(\lambda\pi)+\sigma^2} \\ &\quad = \frac{\eta_2(s,\sigma)(s^2+2s\sigma\cos(\lambda\pi)+\sigma^2)-\eta_3(s,\sigma)s}{(s^2+2s\sigma\cos(\lambda\pi)+\sigma^2)(s^2+2s\sigma\cos(\lambda\pi)+\sigma^2+\eta_3(s,\sigma))} \\ &\quad = \frac{\frac{\eta_2(s,\sigma)}{\sigma^2}((\frac{s}{\sigma})^2+2\frac{s}{\sigma}\cos(\lambda\pi)+1) - \frac{\eta_3(s,\sigma)}{\sigma^3}\frac{s}{\sigma}}{((\frac{s}{\sigma})^2+2\frac{s}{\sigma}\cos(\lambda\pi)+1)((\frac{s}{\sigma})^2+2\frac{s}{\sigma}\cos(\lambda\pi)+1+\frac{\eta_3(s,\sigma)}{\sigma^2})}. \end{aligned} \tag{3.40}$$

Now, when $0 < -s \le \sigma$ we have $0 < |s| \le |\sigma|$ and from (3.38) it follows that $\eta_2(s,\sigma)/\sigma^2 = O(1)$, $\eta_3(s,\sigma)/\sigma^3 = O(1)$ and $\eta_3(s,\sigma)/\sigma^2 \to 0$ as $(s,\sigma)\to(0,0)$. Moreover, since $\lambda \in (0,2)\backslash\{1\}$, we have

$$x^2+2x\cos(\lambda\pi)+1 \;\ge\; \sin^2(\lambda\pi) \;>\; 0 \quad \text{for all } \; x\in\mathbb{R}\,.$$

Combining all these facts with (3.40) shows that the first term in (3.39) is bounded as $(s,\sigma)\to(0,0)$. Since $\widehat{F}_D$ is a bounded function it follows that $\widehat{L}_D(s,\sigma) - \widehat{K}_D(s,\sigma)$ is bounded for $-\Lambda \le s \le 0 \le \sigma \le \Lambda$.

For $-\Lambda \le \sigma \le 0 \le s \le \Lambda$ the result follows analogously.

□

We shall analyse the equation (3.27) in the space, $L^2[-\Lambda,\Lambda]$, of 2Λ-periodic functions with the norm $\|v\|_{L^2[-\Lambda,\Lambda]} = \{\int_{-\Lambda}^{\Lambda} |v(\sigma)|^2 d\sigma\}^{1/2}$. This allows us to cover the Neumann and Dirichlet problems in a unified setting. (There is a corresponding theory in the space $L^\infty[-\Lambda,\Lambda]$ which applies to the Dirichlet problem but not to the Neumann problem.) The next result follows directly from Theorem 3.5.

Corollary 3.6 *For $B = D$ or N, $\widehat{\mathcal{L}}_B - \widehat{\mathcal{K}}_B$ is a compact operator on $L^2[-\Lambda,\Lambda]$.*

Proof The kernel of $\widehat{\mathcal{L}}_B - \widehat{\mathcal{K}}_B$ is $(\widehat{L}_B - \widehat{K}_B)(s,\sigma)$ which, from Theorem 3.5, is a bounded function and the result follows from [19, page 326].

□

The remainder of this section is devoted to proving the well-posedness of (3.27) in $L^2[-\Lambda,\Lambda]$. This is done in Corollary 3.9. Since $\widehat{\mathcal{L}}_B$ is a compact perturbation of $\widehat{\mathcal{K}}_B$, the key part of the proof of Corollary 3.9 is contained in the following theorem, which is of key importance also when we come to the numerical analysis in §4.

Theorem 3.7 *For $B = D$ or N, $(I + \widehat{\mathcal{K}}_B)^{-1}$ exists and is bounded on $L^2[-\Lambda,\Lambda]$.*

Proof Since it follows standard procedures for dealing with Mellin convolution operators we will be brief. More detail is in [8]. The first step is to write the operator $v \mapsto (I + \widehat{\mathcal{K}}_B)v$ on $L^2[-\Lambda,\Lambda]$ as two coupled convolution operators on $[0,\Lambda]$. For $(w_1, w_2) \in L^2[0,\Lambda] \times L^2[0,\Lambda]$ we introduce the norm $\|(w_1,w_2)\| = \{\|w_1\|^2_{L^2[0,\Lambda]} + \|w_2\|^2_{L^2[0,\Lambda]}\}^{1/2}$. Also we define the map $\Pi : L^2[-\Lambda,\Lambda] \to L^2[0,\Lambda] \times L^2[0,\Lambda]$ by

$$\Pi v := (v_1, v_2), \text{ where } v_1(s) = v(-s) + v(s) \quad \text{and} \quad v_2(s) = v(-s) - v(s), \quad s \in [0,\Lambda].$$

Clearly Π is a bijection and $\|\Pi v\|^2 = 2\|v\|^2_{L^2[-\Lambda,\Lambda]}$. Moreover, an elementary calculation using (3.33) and (3.34) and the analogous kernels for $B = N$ (see [8] for details) shows that

$$\Pi \widehat{\mathcal{K}}_B = \tilde{\mathbb{K}}_B \Pi, \quad B = D \text{ or } N. \tag{3.41}$$

Here $\tilde{\mathbb{K}}_B$ is the matrix operator

$$\tilde{\mathbb{K}}_B = \begin{pmatrix} \widetilde{\mathcal{K}}_B & 0 \\ 0 & -\widetilde{\mathcal{K}}_B \end{pmatrix},$$

and $\widetilde{\mathcal{K}}_B$ is the *Mellin convolution* operator on $L^2[0,\Lambda]$ defined by

$$(\widetilde{\mathcal{K}}_B v)(s) = \int_0^\Lambda \tilde{\kappa}_B(s/\sigma) v(\sigma) \frac{d\sigma}{\sigma},$$

with kernels

$$\tilde{\kappa}_D(s) = -\frac{\sin(\lambda\pi)}{\pi} \frac{s}{1 - 2s\cos\lambda\pi + s^2}, \qquad \tilde{\kappa}_N(s) = \frac{\sin(\lambda\pi)}{\pi} \frac{1}{1 - 2s\cos\lambda\pi + s^2}\ .$$

Hence, for all $v \in L^2[-\Lambda,\Lambda]$, we have

$$(I + \widehat{\mathcal{K}}_B)v = \Pi^{-1}(I + \tilde{\mathbb{K}}_B)\Pi v. \tag{3.42}$$

It can be shown, using Mellin integral transform techniques, that $\|\widetilde{\mathcal{K}}_B\|_{L^2[0,\Lambda]} < 1$ (see [8]). Hence by Banach's lemma $I \pm \widetilde{\mathcal{K}}_B$ has a bounded inverse on $L_2[0,\Lambda]$ and the result follows from (3.42). □

Corollary 3.6 and Theorem 3.7 can now be combined to obtain the well-posedness of (2.12), via the Fredholm alternative. The proof requires the following assumption.

Assumption 3.8 *The homogeneous version of (2.12) has only the trivial solution, i.e.*

$$(I + \widehat{\mathcal{L}}_B)\widehat{u} = 0 \ \Rightarrow\ \widehat{u} = 0, \quad \textit{for } \widehat{u} \in L^2[-\Lambda,\Lambda].$$

A proof of this assumption requires (a) uniqueness results for the PDE $\Delta^* + \nu^2 - 1/4$ on the manifolds M and $S^2\backslash\{M \cup \ell\}$ and (b) jump relations for various layer potentials on ℓ. These can be easily established when ℓ is smooth using, for example, the results in [12] to obtain the jump relations (see [8]). It is expected that Assumption 3.8 will continue to hold when ℓ has corners (just as the corresponding statement for the planar Helmholtz equation also holds for corner domains) but we do not attempt to prove it here.

Corollary 3.9 *For $B = D$ or N, suppose that Assumption 3.8 holds. Then $(I+\widehat{\mathcal{L}}_B)^{-1}$ exists and is bounded on $L^2[-\Lambda,\Lambda]$.*

Proof Using Theorem 3.7 the left-hand equation in (3.27) can be rewritten as

$$(I + (I + \widehat{\mathcal{K}}_B)^{-1}(\widehat{\mathcal{L}}_B - \widehat{\mathcal{K}}_B))\widehat{u} = (I + \widehat{\mathcal{K}}_B)^{-1}\widehat{b}_B. \tag{3.43}$$

Since, by Corollary 3.6, $(I + \widehat{\mathcal{K}}_B)^{-1}(\widehat{\mathcal{L}}_B - \widehat{\mathcal{K}}_B)$ is a compact operator, it follows from the Fredholm alternative that (3.43) has a unique solution. It also follows that the operator on the left-hand side of (3.43) has a bounded inverse. Therefore,

$$\|\widehat{u}\|_{L^2[-\Lambda,\Lambda]} \leq C\|(I + \widehat{\mathcal{K}}_B)^{-1}\widehat{b}\|_{L^2[-\Lambda,\Lambda]} \leq C\|\widehat{b}_B\|_{L^2[-\Lambda,\Lambda]},$$

and the result follows. □

Remark 3.10 *If the cone Ξ contains more than one lateral edge, then the contour ℓ will contain several corners. All the results of this subsection remain true in this case. In particular the analogue of Corollary 3.9 ensures the well-posedness of (3.27), or equivalently (2.12) in the multiple corner case. The proof is entirely analogous to the proof above, except that a pair of coupled Mellin convolution equations local to each corner has to be considered. Such systems are standard – see e.g. [9].*

4 Numerical Method

In this section we shall discuss piecewise polynomial collocation methods for (3.27) and obtain their convergence, using the results of §3. We also describe briefly its efficient implementation. The performance of this scheme will be illustrated in §5.

The basic collocation scheme is entirely standard, so we will be brief. First introduce a mesh:

$$-\Lambda = x_0 < x_1 < \ldots < x_m < x_{m+1} < \ldots < x_n = \Lambda\ . \tag{4.1}$$

We assume here that ℓ has a single corner situated at $x_m = 0$ in parameter space and that $n = 2m$. The case of several corners is similar (see Remark 3.10), and a smooth boundary is straightforward (see [8]). We define $I_i = [x_{i-1}, x_i]$ and $h_i = x_i - x_{i-1}$. We assume that for each integer $r \geq 1$, we have chosen, *a priori*, r points: $0 < \xi_1^r < \xi_2^r < \ldots < \xi_r^r < 1$. Then we introduce the approximation space

$$S_n^r[-\Lambda,\Lambda] = \{v \in L^\infty[-\Lambda,\Lambda] : v|_{I_i} \in P_r\}\ , \tag{4.2}$$

where P_r denotes the set of polynomials of order $r \geq 1$ (degree $r-1$). Also, on each I_i, we define the r collocation points $x_{ij}^r = x_{i-1} + h_i\xi_j^r$ and we define the basis functions of $S_n^r[-\Lambda,\Lambda]$

by

$$\phi_{ij}(x) = \begin{cases} \displaystyle\prod_{\substack{1\le k\le r\\ k\neq j}} \frac{x - x^r_{ik}}{x^r_{ij} - x^r_{ik}} \chi_i(x), & \text{when} \quad r > 1 \\ \chi_i(x) & \text{when} \quad r = 1 \ , \end{cases}$$

for $j = 1, \ldots, r$ and $i = 1, \ldots, n$, where χ_i is the characteristic function on I_i. Clearly $\phi_{ij}|_{I_i} \in P_r$ and $\phi_{ij}(x_{i'j'}) = \delta_{ii'}\delta_{jj'}$.

In the collocation method for (3.27), we seek an approximate solution

$$\widehat{u}_n(s) := \sum_{i=1}^{n} \sum_{j=1}^{r_i} \mu_{ij}\phi_{ij}(s),$$

where μ_{ij} are chosen so that the residual vanishes at the collocation points:

$$\mu_{i'j'} + \sum_{i=1}^{n} \sum_{j=1}^{r_i} \mu_{ij} \int_{I_i} \widehat{L}_B(x^r_{i'j'}, \sigma)\phi_{ij}(\sigma)d\sigma = \widehat{b}_B(x^r_{i'j'}) \ , \text{ for } \ i' = 1, \ldots, n \ , \ j' = 1, \ldots, r \ , \quad (4.3)$$

Equivalently,

$$(I + \widehat{\mathcal{P}}_n\widehat{\mathcal{L}}_B)\widehat{u}_n = \widehat{\mathcal{P}}_n\widehat{b}_B \ , \quad (4.4)$$

where $\widehat{\mathcal{P}}_n$ denotes the projection onto $S^r_n[-\Lambda, \Lambda]$, defined by interpolation at the collocation points.

Here we restrict to the h method and assume r is fixed. In §5 we briefly discuss $h - p$ methods, where the polynomial degree on some subintervals may increase as the mesh is refined. Thus we adopt the usual *a priori* mesh grading for this type of problem:

$$x_{m\pm i} = \pm(i/m)^q\Lambda \ , \qquad \text{for } i = 0, \ldots, m, \quad (4.5)$$

where $q \geq 1$ is the grading exponent.

The stability of the collocation scheme now follows from the analysis in §3 and known results on the stability of collocation for Mellin convolution equations [13] – see also [9, 15]. To state this result we need to concept of a *modification parameter* $i* \geq 0$. Given such a parameter, the corresponding *modified collocation scheme* is exactly the same as that described in (4.3) when $i* = 0$. But when $i* > 1$, $\widehat{u}_n$ is set to 0 on each of the subintervals I_i , $i = m-i*+1, \ldots, m+i*$ and (4.3) are required to hold only for $i' \notin \{m-i*+1, \ldots m+i*\}$. (In other words, the collocation solution is set to 0 on each of the $2i*$ subintervals nearest the corner.) For notational convenience we shall continue to write the collocation equations as (4.4), thus suppressing $i*$ from the notation.

Theorem 4.1 *For $B = D$ or N there exists a modification parameter $i*$ and a constant $C > 0$ such that for all n sufficiently large,*

$$\|(I + \widehat{\mathcal{P}}_n\widehat{\mathcal{L}}_B)v_n\|_{L^2[-\Lambda,\Lambda]} \geq C\|v_n\|_{L^2[-\Lambda,\Lambda]},$$

for all $v_n \in S^{\boldsymbol{r}}_n[-\Lambda, \Lambda]$.

Proof We shall show that, for each $\epsilon > 0$ there exists a modification $i*$ such that for n sufficiently large

$$\|(I - \widehat{\mathcal{P}}_n)\widehat{\mathcal{L}}_B v_n\|_{L^2[-\Lambda,\Lambda]} \leq \epsilon \|v_n\|_{L^2[-\Lambda,\Lambda]}, \tag{4.6}$$

for all $v_n \in S_n^{\boldsymbol{r}}[-\Lambda, \Lambda]$. Then, since $I + \widehat{\mathcal{P}}_n\widehat{\mathcal{L}}_B = (I + \widehat{\mathcal{L}}_B) - (I - \widehat{\mathcal{P}}_n)\widehat{\mathcal{L}}_B$, the required result follows from standard operator theory and Corollary 3.9.

To prove (4.6), first we use the triangle inequality to obtain, for $v_n \in S_n^{\boldsymbol{r}}[-\Lambda, \Lambda]$,

$$\|(I - \widehat{\mathcal{P}}_n)\widehat{\mathcal{L}}_B v_n\|_{L^2[-\Lambda,\Lambda]} \leq \|(I - \widehat{\mathcal{P}}_n)\widehat{\mathcal{K}}_B v_n\|_{L^2[-\Lambda,\Lambda]} + \|(I - \widehat{\mathcal{P}}_n)(\widehat{\mathcal{L}}_B - \widehat{\mathcal{K}}_B)v_n\|_{L^2[-\Lambda,\Lambda]}. \tag{4.7}$$

Now recall that $\widehat{\mathcal{P}}_n$ projects to zero on the $2i*$ intervals nearest 0. Thus

$$\begin{aligned} \|(I - \widehat{\mathcal{P}}_n)(\widehat{\mathcal{L}}_B - \widehat{\mathcal{K}}_B)v_n\|^2_{L^2[-\Lambda,\Lambda]} &\leq \|(\widehat{\mathcal{L}}_B - \widehat{\mathcal{K}}_B)v_n\|^2_{L^2[x_{m-i*},x_{m+i*}]} \\ &+ \|(I - \widehat{\mathcal{P}}_n)(\widehat{\mathcal{L}}_B - \widehat{\mathcal{K}}_B)v_n\|^2_{L^2([-\Lambda,\Lambda]\setminus[x_{m-i*},x_{m+i*}])}. \end{aligned} \tag{4.8}$$

Since $(\widehat{\mathcal{L}}_B - \widehat{\mathcal{K}}_B)$ is compact from $L^2[-\Lambda, \Lambda]$ to $C[-\Lambda, \Lambda]$ the first term on the right-hand side of (4.8) may be estimated by

$$\|(\widehat{\mathcal{L}}_B - \widehat{\mathcal{K}}_B)v_n\|^2_{L^2[x_{m-i*},x_{m+i*}]} \leq 2x_{m+i*}\|(\widehat{\mathcal{L}}_B - \widehat{\mathcal{K}}_B)v_n\|^2_{L^\infty[x_{m-i*},x_{m+i*}]} \leq Cn^{-q}\|v_n\|^2_{L^2[x_{m-i*},x_{m+i*}]}. \tag{4.9}$$

Moreover, introduce $\widehat{\mathcal{P}}^c_n$ to denote the interpolation projector onto $S_n^{\boldsymbol{r}}[-\Lambda, \Lambda]$ without modification (i.e. $i* = 0$). Then $\widehat{\mathcal{P}}^c_n = \widehat{\mathcal{P}}_n$ on $[-\Lambda, \Lambda]\setminus[x_{m-i*}, x_{m+i*}]$ and the second term on the right-hand side of (4.8) may be estimated by $\|(I - \widehat{\mathcal{P}}^c_n)(\widehat{\mathcal{L}}_B - \widehat{\mathcal{K}}_B)v_n\|^2_{L^2[-\Lambda,\Lambda]}$. Since $(I - \widehat{\mathcal{P}}^c_n)$ is pointwise convergent to 0 on $C[-\Lambda, \Lambda]$ and since $\widehat{\mathcal{L}}_B - \widehat{\mathcal{K}}_B$ is compact from $L^2[-\Lambda, \Lambda]$ to $C[-\Lambda, \Lambda]$ we then have

$$\|(I - \widehat{\mathcal{P}}^c_n)(\widehat{\mathcal{L}}_B - \widehat{\mathcal{K}}_B)v_n\|^2_{L^2[-\Lambda,\Lambda]} \leq o(1)\|v_n\|^2_{L^2[-\Lambda,\Lambda]}. \tag{4.10}$$

By (4.7) - (4.10) we see that to prove (4.6) it is sufficient to prove it with $\widehat{\mathcal{L}}_B$ replaced by $\widehat{\mathcal{K}}_B$.

To do this, we first employ the operators Π and $\tilde{\mathbb{K}}_B$ defined in the proof of Theorem 3.7, as well as the fact that the mesh (4.1) is symmetric about 0, to obtain $\Pi\widehat{\mathcal{P}}_n\widehat{\mathcal{K}}_B = \tilde{\mathbb{P}}_n\tilde{\mathbb{K}}_B\Pi$ where

$$\tilde{\mathbb{P}}_n = \begin{pmatrix} \tilde{\mathcal{P}}_n & 0 \\ 0 & \tilde{\mathcal{P}}_n \end{pmatrix}.$$

with $\tilde{\mathcal{P}}_n$ defined as the restriction of $\widehat{\mathcal{P}}_n$ to functions on $[0, \Lambda]$. Thus, we have $I + \widehat{\mathcal{P}}_n\widehat{\mathcal{K}}_B = \Pi^{-1}(I + \widetilde{\mathbb{P}}\widetilde{\mathbb{K}}_B)\Pi$ and the proof is complete if we show that for all $\epsilon > 0$, there exists a modification $i*$ such that

$$\|(I - \tilde{\mathcal{P}}_n)\tilde{\mathcal{K}}_B v_n\|_{L^2[0,\Lambda]} \leq \epsilon \|v_n\|_{L^2[0,\Lambda]}\ , \tag{4.11}$$

for all $v_n \in S_n^{\boldsymbol{r}}[0, \Lambda]$. However result (4.11) follows from the general results in [15] on numerical methods for Mellin convolution equations. (See Theorem 3.1 there, and the remarks following it. Note that $\tilde{\kappa}_B$ and $\tilde{\kappa}_N$ both satisfy the conditions (A1) and (A2) of [15], with $p = 2$.) See [17], [9], [13] and also [8] for more details about the approximation of solutions of Mellin convolution equations. □

Remark 4.2 *The introduction of the parameter $i*$ is solely a device to prove stability of the collocation method for (2.12) when ℓ contains a corner. No unmodified practical collocation method has ever been observed to be unstable. However the proof that these methods are stable without modification has eluded researchers for 15 years. For this reason and to simplify the presentation we assume that Theorem 4.1 holds for $i* = 0$ (i.e. no modification) for the remainder of this section.*

Theorem 4.1 implies that the collocation equation (4.4) is uniquely solvable for all n sufficiently large. An easy manipulation using the equations (2.12) and (4.4) shows that $(I + \widehat{\mathcal{P}}_n\widehat{\mathcal{L}}_B)(\widehat{\mathcal{P}}_n\widehat{u} - \widehat{u}) = -\widehat{\mathcal{P}}_n\widehat{\mathcal{L}}_B(I - \widehat{\mathcal{P}}_n)\widehat{u})$. Theorem 4.1 then implies

$$\|\widehat{\mathcal{P}}_n\widehat{u} - \widehat{u}_n\|_{L^2[-\Lambda,\Lambda]} \leq C\|\widehat{\mathcal{P}}_n\widehat{\mathcal{L}}_B(I - \widehat{\mathcal{P}}_n)\widehat{u}\|_{L^2[-\Lambda,\Lambda]}. \tag{4.12}$$

After some technical manipulations using properties of $\widehat{\mathcal{L}}_B = \widehat{\mathcal{K}}_B + (\widehat{\mathcal{L}}_B - \widehat{\mathcal{K}}_B)$ it can be shown that the right-hand side of (4.12) can be bounded by a constant multiple of $\|(I - \widehat{\mathcal{P}}_n)\widehat{u}\|_{L^2[-\Lambda,\Lambda]}$ (see [8]). Then the triangle inequality implies:

$$\|\widehat{u} - \widehat{u}_n\|_{L^2[-\Lambda,\Lambda]} \leq C\|(I - \widehat{\mathcal{P}}_n)\widehat{u}\|_{L^2[-\Lambda,\Lambda]}. \tag{4.13}$$

Therefore to obtain convergence rates we need estimates for $\|\widehat{u} - \widehat{\mathcal{P}}_n\widehat{u}\|_{L^2[-\Lambda,\Lambda]}$. These of course depend on the regularity of the solution. To describe this regularity we introduce the weighted Sobolev space for an interval $J \subset \mathbb{R}$. For $k \in \mathbb{N}$ and $\alpha \in \mathbb{R}$

$$L^{2,k}_\alpha(J) = \{v : |x|^{j-\alpha}D^j v \in L^2(J),\ j = 0, 1, \ldots, k\},$$

equipped with the norm $\|v\|_{L^{2,k}_\alpha(J)} = \sum_{j=0}^k \|x^{j-\alpha}D^j v\|_{L^2(J)}$, (see [13]).

Examples 4.3

(i) The function

$$\widehat{u}(x) = C' + C''|x|^\theta, \quad \textit{where} \quad 1/2 < \theta < 1, \tag{4.14}$$

satisfies $\widehat{u}(x) - C' \in L^{2,k}_\alpha[-\Lambda, \Lambda]$ for all $k \geq 0$ and $\alpha < \theta + 1/2$.

(ii) The function

$$\widehat{u}(x) = C|x|^{\theta-1}, \quad \textit{where} \quad 1/2 < \theta < 1, \tag{4.15}$$

satisfies $\widehat{u}(x) \in L^{2,k}_\alpha[-\Lambda, \Lambda]$ for all $k \geq 0$ and $\alpha < \theta - 1/2$.

Remark 4.4 *When we solve the Dirichlet problem for the Laplace equation in the region interior to a planar polygon using the indirect boundary integral method, the solution of the resulting integral equation has its principal singularity in the form (4.14), where the corner is at $x = 0$ and $\theta = 1/(1 + |\chi|)$, where$(1 - \chi)\pi$ is the angle between the tangents at the corner ($\chi \in (-1, 1)\backslash\{0\}$). When we solve the Neumann problem with the same geometry again using the indirect boundary method the density has its principal singularity in the form (4.15), again with $\theta = 1/(1 + |\chi|)$ (see e.g [11], [17], [13]).*

Since the integral operator in the spherical boundary integral equations has a principal part which coincides with the Laplace integral operator we conjecture that the solutions of our integral equations have the same principal singularity as identified in Examples 4.3 (i) and (ii). The numerical results in §5 support this conjecture.

Following Remark 4.4, in [8] we prove estimates for $\|(I-\widehat{\mathcal{P}}_n)\widehat{u}\|_{L^2[-\Lambda,\Lambda]}$ under assumptions which encapsulate Examples 4.3(i) and (ii). Combining this with (4.13) the final result is (see [8]):

Theorem 4.5 *(i) Suppose that $B = D$ and that the exact solution to (3.27) satisfies $\widehat{u} - C' \in L^{2,r}_\alpha[-\Lambda,\Lambda]$ with $1 < \alpha < 3/2$, then for sufficiently large n the collocation method described by (4.4) converges with error*

$$\|\widehat{u} - \widehat{u}_n\|_{L^2[-\Lambda,\Lambda]} = Cn^{-r}\|\widehat{u} - C'\|_{L^{2,r}_\alpha[-\Lambda,\Lambda]} \quad as \quad n \to \infty, \tag{4.16}$$

provided the grading parameter $q \geq \max\{r/\alpha, 1\}$.

(ii) Suppose that $B = N$ and that the exact solution to (3.27) satisfies $\widehat{u} \in L^{2,r}_\alpha[-\Lambda,\Lambda]$ for some $0 < \alpha < 1/2$, then for sufficiently large n the collocation method described by (4.4) converges with error

$$\|\widehat{u} - \widehat{u}_n\|_{L^2[-\Lambda,\Lambda]} = Cn^{-r}\|\widehat{u}\|_{L^{2,r}_\alpha[-\Lambda,\Lambda]} \quad as \quad n \to \infty, \tag{4.17}$$

provided the grading parameter $q \geq r/\alpha$.

The implementation of the collocation method (4.3) requires the efficient calculation of the stiffness matrix entries

$$\widehat{\mathbb{L}}_{i'j',ij} := \int_{I_i} \widehat{L}_B(x^r_{i'j'}, \sigma)\phi_{ij}(\sigma)d\sigma. \tag{4.18}$$

Each evaluation of the kernel $\widehat{L}_B$ in (4.18) requires an evaluation of (the derivative) of the Legendre function with complex index (see (3.28), (3.29)). We do this by integrating Legendre's differential equation using a Runge-Kutta method – details are in [8]. Thus efficient quadrature methods for (4.18) are of the utmost importance. This is especially true when we remember that (2.12) needs to be solved many times over (for different values of ν on the imaginary axis) in order to allow the approximate integration of (1.4). The key difficulty in evaluating (4.18) is the singularity which arises when $i' = i$. (This is strongest when I_i contains the origin in parameter space, corresponding to the corner on ℓ.) In [8] a detailed study of quadrature for (4.18) is carried out. Here we have room to mention only the most useful result from [8]:

Theorem 4.6 *Suppose the collocation points x^r_{ij}, $j = 1, \ldots, r$, are chosen to be the r Gauss-Legendre points on $[0,1]$, shifted to I_i. Then we may approximate (4.18) using Gauss-Legendre quadrature based also at these points. If we do this for all i, i' satisfying*

$$\mathrm{dist}(I'_i, I_i) \geq h_i^{1/(r+2)}, \tag{4.19}$$

then the $O(n^{-r})$ convergence rate reported in Theorem 4.5 continues to hold.

Since ϕ_{ij} vanishes at all the points x^r_{ik}, except $k = j$, the implementation of the rule in Theorem 4.6 requires only one kernel evaluation and (4.19) shows that this can be done for most of the matrix as the mesh is refined. It also turns out that even when (4.19) is not satisfied, rules with $O(\log(n))$ kernel evaluations can be employed and the $O(n^{-r})$ rate in Theorem 4.5 remains unperturbed – for more details see §5 and also [8].

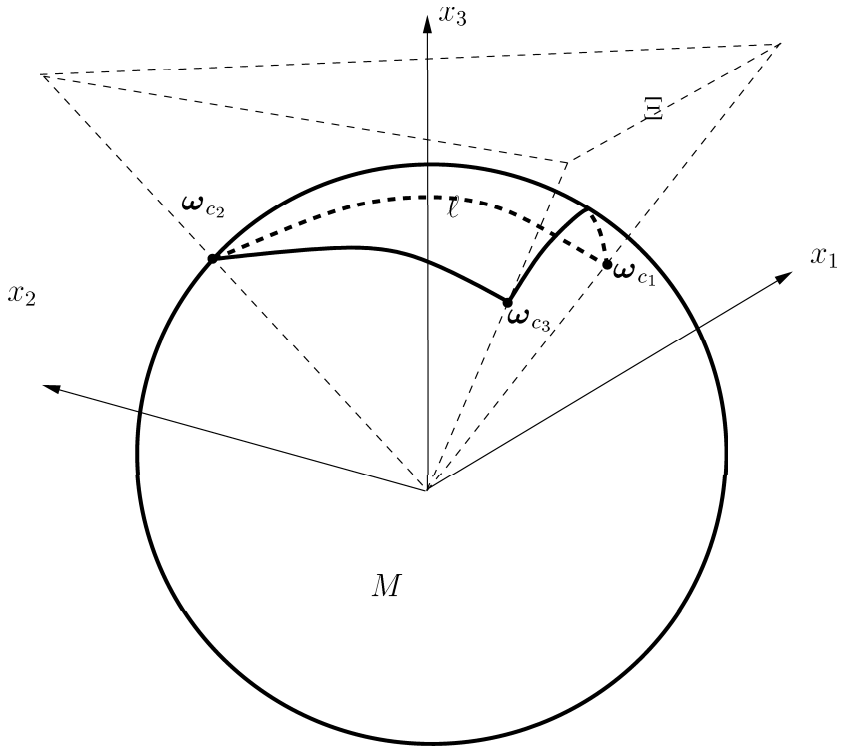

Figure 4: The contour ℓ associated with a trihedral cone

5 Numerical Results

We shall illustrate the performance of the numerical method described above in the case of the diffraction of acoustic waves by a trihedral cone. In the asymptotics literature this is an unsolved *canonical problem* - i.e. it is a relatively simple geometry which often occurs in applications, but there is no known closed form expression for the diffraction coefficients.

Our trihedral cone is determined by three rays which emanate from the origin and pass through the points $\boldsymbol{\omega}_{c_i} \in S^2$, $i = 1, 2, 3$, which are specified by spherical polar coordinates $(\theta^*, 0), (\theta^*, 2\pi/3)$ and $(\theta^*, 4\pi/3)$ respectively, where $\cos\theta^* = 1/\sqrt{3}$. The conical scatterer Ξ has its surface composed of the three planar segments determined by each pair of rays and the contour ℓ is made up of three smooth geodesic curves in S^2, with each pair of smooth curves meeting at an angle of $\pi/2$ at one of the points $\boldsymbol{\omega}_{c_i}$. The geometry is depicted in Fig. 4. The contour ℓ is drawn in bold.

Throughout the computations we used collocation at the Gauss points of subintervals. For the evaluation of the boundary integrals (4.18), we used Gauss quadrature at the collocation points in the "far field", i.e. when i, i' satisfy (4.19). When (4.19) does not hold we increase the number of quadrature points, d, logarithmically. More precisely, we choose d to be the smallest integer satisfying

$$d \geq \frac{(r+1)\log(n)}{2\log(2)}.$$

Note that for this geometry, when $\boldsymbol{\omega}, \boldsymbol{\omega}'$ lie on the same edge of the geodesic triangle ℓ then $L_B(\boldsymbol{\omega}, \boldsymbol{\omega}') = 0$. Hence one third of the matrix entries are zero. Included in these zero entries are the integrals that occur when the observation point lies in the interval of integration. Note

that our procedure uses only one kernel evaluation for most matrix entries, as mentioned in §4. We shall see that our numerical results coincide with the theoretical predictions of Theorem 4.5.

Our first set of results illustrate the accuracy of methods for solving the integral equation (2.12) (equivalently (3.27)) arising from the boundary value problem (2.6). For these tests we set $\boldsymbol{\omega}_0 = -\boldsymbol{\omega}_{c_1}$ and set the parameter $\nu = i$.

The density $\widehat{u}$ in (3.27) is not smooth near the corner. In fact, in the case of the Dirichlet problem, we expect from Remark 4.4 that there exists a constant C' such that, $\widehat{u} - C' \in L^{2,r}_\alpha$, with $\alpha < 7/6$. (This is because for the corners in this example $\chi = 1/2$, so $\theta = 2/3$ and hence $\theta + 1/2 = 7/6$.) When Neumann boundary conditions are prescribed, we expect $\widehat{u} \in L^{2,r}_\alpha$, $\alpha < 1/6$. So for the Dirichlet problem, piecewise constant approximation should yield optimal $O(n^{-1})$ convergence (in the L^2 sense) on a uniform mesh ($q = 1$, cf. Theorem 4.5). On the other hand for the Neumann problem we expect a rate of convergence close to $O(n^{-1/6})$ on a uniform mesh.

To illustrate convergence, for each case we have computed an "exact" solution $\widehat{u}^*$ by using piecewise linear collocation on a mesh with 498 nodes. (To obtain the "exact" Dirichlet solution we grade the mesh towards the corners with $q = 2$ and for the the "exact" Neumann solution, since the optimal grading is rather severe, we only use a grading exponent $q = 3$. Recall the mesh is given in (4.5).) We computed the approximate L^2 error $\mathrm{err}^1_n := \|\widehat{u}^* - \widehat{u}_n\|_2$ using mid-point quadrature with respect to the mesh with n subintervals.

The results are given in Table 1. As expected, a convergence rate of close to $O(n^{-1})$ is observed for the Dirichlet problem and close to $O(n^{-1/6})$ for the Neumann problem.

Table 1: Estimated errors for the piecewise constant collocation method for (3.27) on a uniform mesh

	Dirichlet Problem		Neumann Problem	
n	err^1_n	ratio	err^1_n	ratio
24	9.957E-2		1.609E-3	
48	5.285E-2	1.88	1.530E-3	1.05
96	2.472E-2	2.14	1.229E-3	1.24
192	1.074E-2	2.30	1.077E-3	1.14
384	4.992E-3	2.15	9.589E-4	1.12

As we have shown, mesh grading will improve the rates of convergence, (except in the piecewise constant approximation of the Dirichlet problem case where optimal convergence is obtained using a uniform mesh). Consider the Neumann problem. Because the Neumann solution satisfies, $\widehat{u} \in L^{2,r}_\alpha$, with $\alpha < 1/6$, it can be shown that with $q' \le 6r$ a rate of convergence of $O(n^{-q'/6})$ in the L^2 norm can be attained when a graded mesh is used with grading exponent $q > q'$ for collocation onto piecewise polynomials of order r. We illustrate the correctness of this result with $q = 3$. The results are in Table 2.

Here we find that the Neumann problem now converges with rate close to $O(n^{-1/2})$, as expected. The Dirichlet problem now appears to converge with a superoptimal rate, but this could be expected to subside back to $O(n^{-1})$ asymptotically. These results indicate that our integral equation solver is working as predicted by the theory.

Table 2: Estimated errors for the piecewise constant collocation method for (3.27) on a graded mesh, q=3

	Dirichlet Problem		Neumann Problem	
n	err_n^1	ratio	err_n^1	ratio
24	1.257E-2		6.307E-3	
48	4.948E-3	2.54	6.106E-3	1.03
96	2.147E-3	2.30	4.744E-3	1.29
192	7.842E-4	2.74	3.553E-3	1.34
384	2.442E-4	3.21	2.738E-3	1.30

Our next set of results illustrate the convergence of the approximate solutions to the spherical boundary-value problem (2.6), (2.7). We consider the same problem as above with $\boldsymbol{\omega}_0 = -\boldsymbol{\omega}_c$, and $\nu = i$. In Tables 3 and 4, we tabulate the errors in approximate solutions to (2.6), (2.7) obtained by substituting $u_n(\boldsymbol{\rho}(s), \nu) = \widehat{u}_n(s)$ into (2.8) (in the Dirichlet case) and (2.10) (in the Neumann case) and computing the resulting integral by the Gauss quadrature rule based at the points used in the computation of $\widehat{u}_n$. For illustration we have chosen to observe the solution at the particular observation direction $\boldsymbol{\omega} = (0, 0, -1)$. The error err_n^2 is computed by $|g_n^r(\boldsymbol{\omega}, \boldsymbol{\omega}_0, \nu) - \widetilde{g}^r(\boldsymbol{\omega}, \boldsymbol{\omega}_0, \nu)|$ where $\widetilde{g}^r$ is computed with a large n (= 330) and $q = 3$.

The results illustrate the superconvergence of the method (well-documented in the case of planar problems (e.g. [9, 2, 15]), with close to $O(n^{-2})$ convergence attained for $q = 3$. The extreme gradings needed for optimal convergence of the density may not be needed for the potential, and in fact better than optimal convergence may be obtained because of the smoothness of the fundamental solution away from the boundary ℓ.

We emphasise that the results in Tables 1 - 4 illustrate not only the convergence theory in §4, but also show that the algorithm used to compute the Legendre function with complex index (by applying a Runge-Kutta method to Legendre's differential equation), which is described in detail in [8], is working in a stable manner.

Table 3: Estimated errors for the potential (2.8) using the piecewise constant collocation method (Dirichlet boundary conditions)

	Uniform mesh, q=1		Graded mesh, q=2		Graded Mesh, q=3	
n	err_n^2	ratio	err_n^2	ratio	err_n^2	ratio
12	3.12E-4		3.16E-4		4.69E-4	
24	1.35E-4	2.3	1.35E-4	2.33	1.67E-4	2.8
48	5.46E-5	2.5	4.19E-5	3.23	6.13E-5	2.7
96	2.10E-5	2.6	1.31E-5	3.21	1.98E-5	3.1
192	8.51E-6	2.5	3.78E-6	3.46	5.61E-6	3.5

Our experiments so far have covered only low-order methods but results for higher order are found in [8]. An important point is that, since only one kernel evaluation is needed for

Table 4: Estimated errors for the potential (2.10) using the piecewise constant collocation method (Neumann boundary conditions)

	Uniform mesh, q=1		Graded mesh, q=2		Graded Mesh, q=3	
n	err_n^2	ratio	err_n^2	ratio	err_n^2	ratio
12	6.25E-5		3.74E-5		4.45E-5	
24	2.71E-5	2.3	1.03E-5	3.64	8.14E-6	5.5
48	1.11E-5	2.4	2.92E-6	3.52	3.07E-6	2.7
96	4.53E-6	2.5	7.62E-7	3.82	8.63E-7	3.6
192	1.81E-6	2.5	1.95E-7	3.91	2.26E-7	3.8

most matrix entries *independent* of the order of the basis functions, the cost of implementation does not increase much as the order of the basis functions is increased. This suggests that the $h-p$ version of the boundary element method should be very competitive for this application and our next set of results concern this method.

For fixed $\sigma \in (0,1)$ we define a geometrically graded mesh on $[-\Lambda, \Lambda]$ by

$$x_{m+i} = \sigma^{m-i}\Lambda, \qquad -x_{m-i} = \sigma^{m-i}\Lambda \qquad i = 1, \ldots, m \qquad x_m = 0. \tag{5.1}$$

We seek an approximate solution on the space S_n^r, defined in (4.2). A typical distribution of orders $\mathbf{r}$ in the $h-p$ version of the algorithm would be :

$$r_i = \lceil (m+1-i)\beta \rceil \text{ for } i < m, \;\; r_i = \lceil (i-m)\beta \rceil \text{ for } i > m+1$$

for some fixed parameter $\beta > 0$, where, for $x \in \mathbb{R}$, $\lceil x \rceil$ denotes the smallest integer which is strictly greater that x. On the intervals I_i, $i = m, m+1$ the approximate solution is set to zero. Thus, on intervals close to the corner we approximate the solution on small subintervals, using low order methods, while further away we use higher order on larger subintervals. The maximum order increases linearly with m and hence also with n.

By making use of the fundamental results of Elschner ([14]) for the Laplace case, and combining these with our results in §3, it can be shown [8] that the $h-p$ method is stable. By making further assumptions about the regularity of the solution to (3.27), it can be shown that the $h-p$ method converges exponentially. In Fig. 5 we illustrate the convergence of the $h-p$ method, compared with the piecewise constant and piecewise linear cases for the potentials (2.8) arising from the Dirichlet problem with $\boldsymbol{\omega}_0 = -\boldsymbol{\omega}_{c_1}$, $\boldsymbol{\omega} = (0,0,-1)$ and $\nu = i$.

In these computations, the parameter values $\sigma = 0.25$ and $\beta = 0.5$ were employed in the $h-p$ method. For these results we naively used the r_i-point Gauss-Legendre rule to calculate the matrix entries $\widehat{\mathbb{L}}_{i'j',ij}$, i.e. in this case *all* of the matrix entries were computed using one kernel evaluation. Observe the exponential convergence of the $h-p$ method in Fig. 5.

Finally, in order to illustrate the computations of the diffraction coefficients for this geometry, we shall show graphically how the computed $f(\boldsymbol{\omega}, \boldsymbol{\omega}_0)$ in (1.4) varies for three different incidence directions $\boldsymbol{\omega}_0$, and many observation directions $\boldsymbol{\omega}$ ranging over a subdomain of M. In this illustration we restrict to the Dirichlet problem, we consider the incident directions given in spherical polar coordinates by

$$\boldsymbol{\omega}_0 = (\pi, 0), \;\; (11\pi/12, 0), \text{ and } (5\pi/6, 0), \tag{5.2}$$

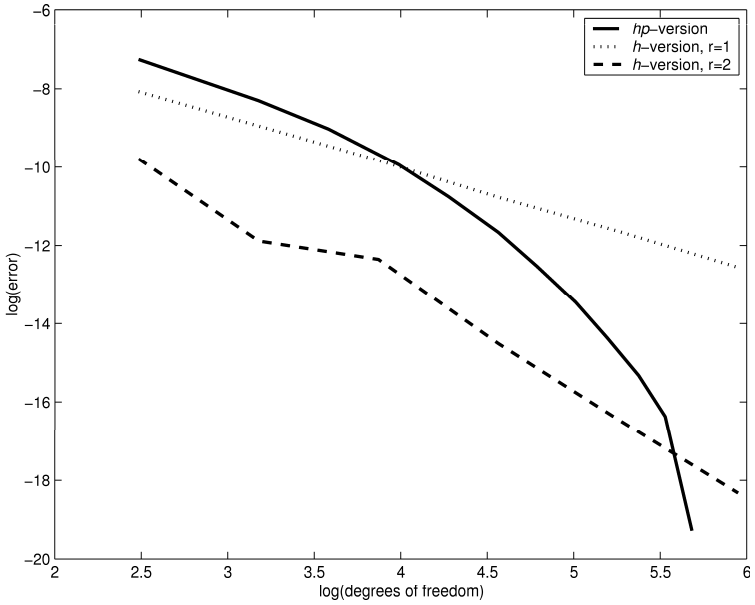

Figure 5: Errors for the potential (2.8) for the h-version and h-p-version of collocation

and a range of observation directions

$$\boldsymbol{\omega} = ((\pi - \theta), \phi) \ , \quad \text{with} \quad 0 \leq \theta \leq \pi/3, \ \ 0 \leq \phi \leq 2\pi. \tag{5.3}$$

In Fig. 6 we illustrate how $|f(\boldsymbol{\omega}, \boldsymbol{\omega}_0)|$ varies as a function of θ and ϕ, for each of the three different incident angles. The quantity $|f(\boldsymbol{\omega}, \boldsymbol{\omega}_0)|$ is plotted on the x_3 axis against the projection of $\boldsymbol{\omega}$ onto the x_1x_2-plane given by: $\boldsymbol{\omega} = (\pi - \theta, \phi) \mapsto (\theta \cos\phi, \theta \sin\phi)$.

Observe in Fig. 6 that when $\boldsymbol{\omega}_0 = (\pi, 0)$, i.e. the incident wave propagates in an "axial" direction, then the magnitude of the diffraction coefficients is smallest in the backscattering direction. This is in qualitative agreement with results for the circular cone [3]. Also note when $\boldsymbol{\omega}_0 = (\pi, 0)$ that if we fix $\theta > 0$ then the distance between $\boldsymbol{\omega} = (\pi - \theta, \phi)$ and the boundary of the nonsingular region, given by $\theta_1(\boldsymbol{\omega}, \boldsymbol{\omega}_0) = \pi$ – see (2.2), is smallest when $\phi = 0, 2\pi/3, 4\pi/3$. At the singular directions f is infinitely large hence the three peaks appear in Fig. 6.

As we vary the angle of incidence the position of the singular directions will vary. In particular it can be shown from (2.2) that for $\boldsymbol{\omega}_0 = (11\pi/12, 0)$ and $(5\pi/6, 0)$, and fixed $\theta > 0$ the distance between $\boldsymbol{\omega}$ and the singular directions is smallest when $\phi = 0$. This explains the faster growth, as θ increases, of $|f(\boldsymbol{\omega}, \boldsymbol{\omega}_0)|$ along $\phi = 0$ (i.e. along the line $x_2 = 0$).

The numerical method used for these computations was the piecewise constant collocation method with $n = 48$ subintervals on a uniform mesh (cf. Theorem 4.5). To produce each picture in Fig. 6 the density in the integral equation (3.27) was approximated for 80 values of ν. Then using these densities we computed the solution to the BVP (2.6), (2.7) for the same 80 values of ν at ~ 800 observation points $\boldsymbol{\omega}$. Therefore $\sim 64,000$ evaluations of the double layer potential were required. The diffraction coefficient f was computed from formula (1.4) by truncation to a finite domain of integration and then applying the trapezoidal rule. The truncation points are chosen according to an analysis of the asymptotics of the integrand in (1.4) and are designed to yield an overall method which converges at the same rate as the method for computing g^r (see [8]).

A colour pdf file of this paper including Fig. 6 may be viewed at:
http://www.maths.bath.ac.uk/∼igg/diffraction.pdf .

References

[1] M. Abramowitz and I.E. Stegun. *Handbook of Mathematical Functions.* Dover Publications, New York, 1965.

[2] K.E. Atkinson. *The Numerical Solution of Integral Equations of the Second Kind.* Cambridge University Press, Cambridge, 1997.

[3] V.M. Babich, D.B. Dement'ev, and B.A. Samokish. On the diffraction of high-frequency waves by a cone of arbitrary shape. *Wave Motion*, 21:203–207, 1995.

[4] V.M. Babich, V.P. Smyshlyaev, D.B. Dement'ev, and B.A. Samokish. Numerical calculation of the diffraction coefficients for an arbitrarily shaped perfectly conducting cone. *IEEE Trans. Antennas & Propagation*, 44:740–747, 1996.

[5] V.M. Babich, D.B. Dement'ev, B.A. Samokish, and V.P. Smyshlyaev. On evaluation of the diffraction coefficients for arbitrary "nonsingular" directions of a smooth convex cone. *SIAM J. Appl. Math.*, 60:536–573, 2000.

[6] V.M. Babič and V.S. Buldryev. *Short-Wave-Length Diffraction Theory.* Springer-Verlag, Berlin, 1991.

[7] J.J. Bowman, T.B.A. Senior , and P.L.E. Uslenghi. *Electromagnetic and Acoustic Scattering by Simple Shapes.* North-Holland, Amsterdam, 1969. Revised 1987.

[8] B.D. Bonner. *Calculating Conical Diffraction Coefficients.* PhD thesis, University of Bath, 2003.

[9] G.A. Chandler and I.G. Graham. Product integration-collocation methods for noncompact integral operator equations. *Math. Comp.*, 50:125–138, 1988.

[10] D. Colton and R. Kress. *Inverse Acoustic and Electromagnetic Scattering Theory.* Springer-Verlag, New York, 1992.

[11] M. Costabel and E.P. Stephan. Boundary integral equations for mixed boundary value problems in polygonal domains and Galerkin approximation. In *Mathematical Models and Methods in Mechanics*, volume 15, pages 175–251. Banach Centre Publications, PWN, Warsaw, 1985.

[12] R. Duduchava. Boundary value problems on a smooth surface with smooth boundary. *Universität Stuttgart, Preprint 2002-5*, 1–19, 2002.

[13] J. Elschner. On spline collocation for convolution equations. *Integral Equations and Oper. Theory*, 12:486–510, 1989.

[14] J. Elschner. The h-p-version of spline approximation methods for Mellin convolution equations. *J. Integral Equations and Appl.*, 5(1):47–73, 1993.

[15] J. Elschner and I.G. Graham. Numerical methods for integral equations of Mellin type. *J. Comp. Appl. Math.*, 125:423–437, 2000.

[16] A. Erdelyi, M. Magnus, F. Oberhettinger, and F.G. Tricomi. *Tables of Integrals Transforms, Vol. 1.* McGraw-Hill, New York, 1954.

[17] I.G. Graham and G.A. Chandler. High-order methods for linear functionals of solutions of second kind integral equations. *SIAM J. Numer. Anal.*, 25:1118–1137, 1988.

[18] E.W. Hobson. *The Theory of Spherical and Ellipsoidal Harmonics.* Cambridge University Press, Cambridge, 1931.

[19] L.V. Kantorovich and G.P. Akilov. *Functional Analysis.* Pergamon, Oxford, 1982.

[20] J.B. Keller. Diffraction by a convex cylinder. *IRE Trans. Ant. Prop.*, 4:312–321, 1956.

[21] J.B. Keller. The geometrical theory of diffraction. *J. Opt. Soc. Amer.*, 52:116–130, 1962.

[22] J.R. Rice. On the degree of convergence of nonlinear spline approximation. In I.J. Schoenberg, editor, *Approximation with Special Emphasis on Spline Functions.* Academic Press, New York, 1969.

[23] V.P. Smyshlyaev. Diffraction by conical surfaces at high frequencies. *Wave Motion*, 12:329–339, 1990.

[24] V.P. Smyshlyaev. The high-frequency diffraction of electromagnetic waves by cones of arbitrary cross-sections. *SIAM J. Appl. Math.*, 53:670–688, 1993.

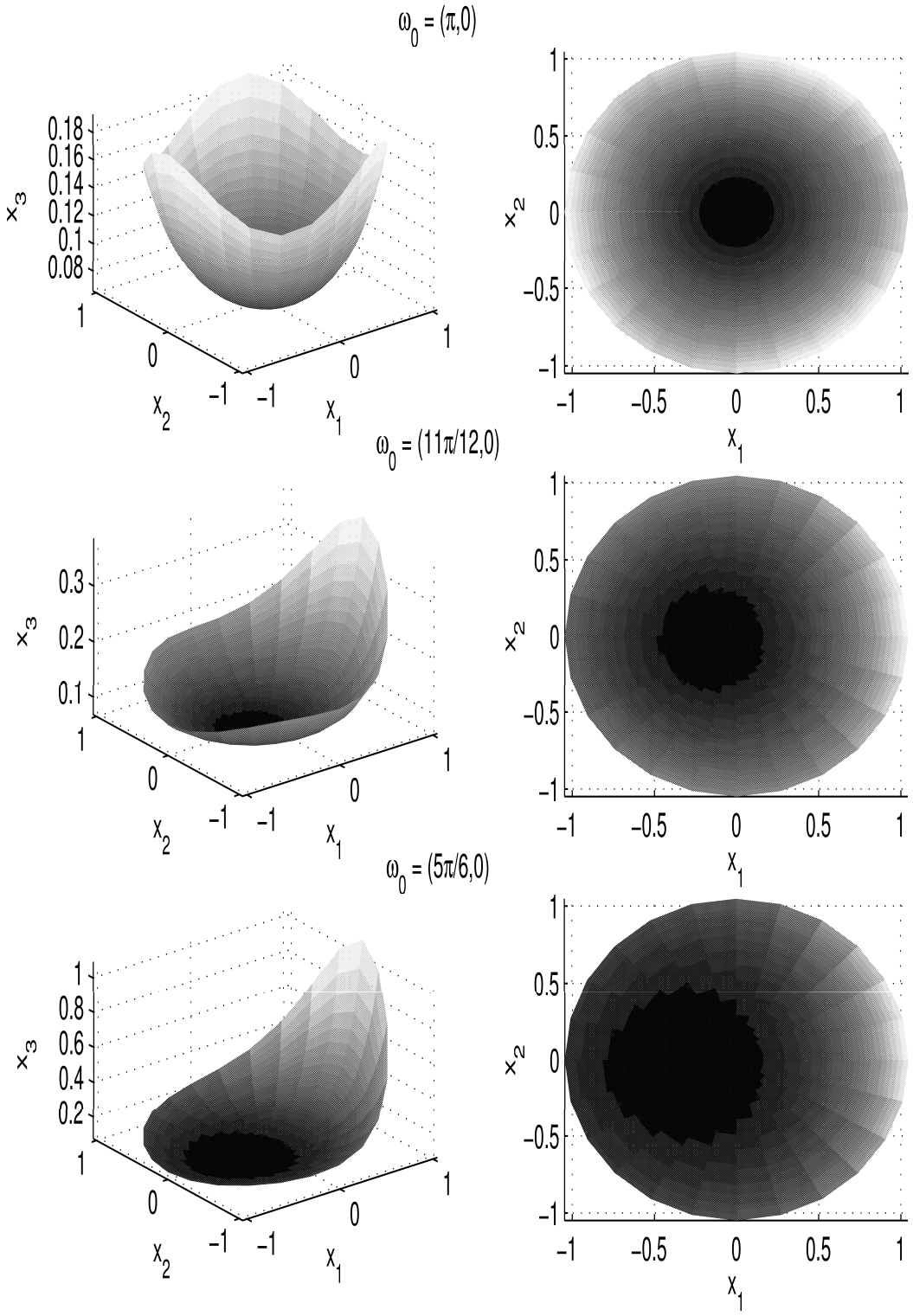

Figure 6: Diffraction coefficients for a trihedral cone